

**DESIGN AND DEVELOPMENT OF HARDWARE PLATFORM FOR FULLY-ASSISTIVE LOWER LEG
EXOSKELETON**

By

Bryan Bonnici
Bachelor of Engineering
Ryerson University, 2013

A thesis

presented to Ryerson University

in partial fulfillment of the
requirements for the degree of

Master of Applied Science

in the Program of

Electrical and Computer Engineering

Toronto, Ontario, Canada

© Bryan Bonnici, 2017

AUTHOR'S DECLARATION

AUTHOR'S DECLARATION FOR ELECTRONIC SUBMISSION OF A THESIS

I hereby declare that I am the sole author of this thesis. This is a true copy of the thesis, including any required final revisions, as accepted by my examiners.

I authorize Ryerson University to lend this thesis to other institutions or individuals for the purpose of scholarly research.

I further authorize Ryerson University to reproduce this thesis by photocopying or by other means, in total or in part, at the request of other institutions or individuals for the purpose of scholarly research.

I understand that my thesis may be made electronically available to the public.

ABSTRACT

DESIGN AND DEVELOPMENT OF HARDWARE PLATFORM FOR FULLY-ASSISTIVE LOWER LEG EXOSKELETON

Bryan Bonnici

Master of Applied Science, Electrical and Computer Engineering, Ryerson University, 2017.

The abundance of cheap, portable computing has allowed for complex applications of robotics, especially in the medical rehabilitation field. The emergence of wearable robotics which simulate the movement of healthy individuals is seen as a new option for treating and rehabilitating individuals with paraplegia and other motor disorders.

This thesis presents the design and implementation of a miniaturized, low-power, extensible hardware platform for control of a fully-assistive lower-body exoskeleton. A preliminary ARM Cortex-M4-based control platform using modular COTS parts was developed and implemented in a medical exoskeleton (the Bionik Laboratories' ARKE) and was evaluated through human medical trials. Clinical feedback was used to drive the design of a new platform. A functional prototype of the design was constructed and retrofitted onto an exoskeleton. Data acquisition and MATLAB was then used to evaluate and compare the performance of the two designs. A size reduction of 29% is achieved.

ACKNOWLEDGEMENTS

Thank you to my graduate supervisor, Dr. Kaamran Raahemifar for providing me the opportunity to study with him and opening the pathway for my future. Without his assistance I truly could not have succeeded to the level I have today.

Thank you to Michal Prywata, Peter Bloch, Amir Takhmar, Nabeel Ahmed and the whole Bionik family for welcoming me into their circle, allowing me to collaborate, and letting me spend time researching with the ARKE.

Thank you to my professors, especially Dr. Vadim Geurkov, Dr. Lev Kirischian, and Dr. Gosha Zywno for their advice and direction.

Thank you to all my friends, especially my graduate colleagues, Brian Battaglia, Steve Chui, Omar Alejandro Rodriguez, Steve Jones, Jean Claude Clarke, Anna Leschenko, Daniel “Freebird” Adarve, Isuru Weerasekera, and last but definitely not least, Nik Trutiak for their ongoing support.

Thank you to my family, who kept me well fed.

Thank you to Goran Slavkovic, Sasko Trajcevski and the Rams Water Polo club, who kept me on my toes.

Last but not least, I would like to thank Ryerson University and the Faculty of Engineering and Architectural Science for their financial support.

DEDICATION

I dedicate this thesis to my mother, Mercedes Salvador, for inspiring me to give people their lives back.

TABLE OF CONTENTS

Author's Declaration.....	ii
Abstract.....	iii
Acknowledgements.....	iv
Dedication.....	v
List of Tables	ix
List of Figures.....	x
List of Appendices	xii
1 Introduction	1
1.1 Motivation	3
1.2 Objectives.....	4
1.3 Author's Contribution	5
1.4 Thesis Layout	6
1.5 Background	7
1.5.1 State of the art	7
1.5.2 Efficacy of Robotic Orthoses.....	11
1.5.3 Gait Cycle and Walking.....	11
1.5.4 Forward Kinematics and Trajectory	12
1.5.5 Motor Control	16
2 Platform Design.....	18
2.1 Introduction	18
2.2 Collaborative work with Bionik Laboratories.....	18
2.3 The ARKE.....	19
2.3.1 Firmware Overview	21
2.3.2 Application Overview	22
2.4 Preliminary Design.....	24
2.4.1 Microcontroller	26
2.4.2 Wireless Interface	27
2.4.3 IMU.....	28
2.4.4 Servomotor Drives	28
2.4.5 Summary of Preliminary Design	29
2.5 Shortcomings of Preliminary Design	30

2.5.1	Resilience	30
2.5.2	Extensibility	30
2.5.3	Signal Integrity.....	31
2.5.4	Power Architecture	32
2.5.5	Design Conclusions for Preliminary Design.....	33
2.6	The Integrated Design	34
2.6.1	Design Requirements	34
2.6.2	Power Architecture	38
2.6.3	Logic Architecture	44
2.6.4	Block Diagrams	50
2.6.5	PCB Layout and Model	51
2.7	Summary	54
3	Fabrication and Test of Integrated Design	55
3.1	Introduction	55
3.2	Validation Method.....	55
3.3	Design Verification	56
3.4	Vendor Selection	56
3.5	Bare Board Inspection and Test	57
3.6	PCB Assembly	59
3.7	PCB Post-Assembly Inspection	60
3.8	PCB Post-Assembly Electrical Test.....	63
3.9	Unit Test and Integration.....	63
3.9.1	Initial Power On.....	63
3.9.2	Power Supply Verification.....	64
3.10	Additional Peripherals.....	66
3.10.1	Foot Sensors.....	66
3.10.2	System Control.....	67
3.10.3	Bluetooth Configuration	68
3.11	Flashing	69
3.12	System Integration.....	69
3.13	Conclusion.....	69
4	Experiment.....	70

4.1	Introduction	70
4.2	Experimental Setup	70
4.3	Trial Procedure	70
4.4	Data Collection and Post Processing.....	71
4.5	Summary	72
5	Experimental Results and Discussion.....	73
5.1	Introduction	73
5.2	Performance data.....	73
5.3	Size Analysis	76
5.4	Summary	77
6	Conclusions and Future Works.....	78
6.1	Conclusions	78
6.2	Improvements	78
6.3	Recommendations and Future Works	79
	Appendices.....	83
	References	92
	Glossary	102

LIST OF TABLES

Table 1.1: Life expectancies of persons with SCI [6].....	1
Table 1.2: Comparison of FDA approved lower body exoskeletons.....	10
Table 2.1 Comparison of Modular vs Integrated designs	33
Table 2.2: Device-level requirements for Integrated Design.....	35
Table 2.3: Mechanical Requirements for Integrated Design	36
Table 2.4: Communication Requirements for Integrated Design	36
Table 2.5: Power Requirements for Integrated Design.....	37
Table 2.6: Processing Requirements for Integrated Design.....	37
Table 2.7: Power Budget Table for Integrated logic board.	39
Table 2.8: Heat analysis of LDO regulators of Integrated Design	41
Table 2.9: Microcontroller Specification [50]	44
Table 2.10: Expansion Port and Console Header Signal Mappings	46
Table 2.11: Dimensions of Integrated Design	54
Table 2.12: Surface Area and Volume of Integrated Design.....	54
Table 3.1: Results of electrical test on unpopulated PCBs	58
Table 3.2: Results of Post-assembly PCB testing.....	63
Table 3.3: Summary of Power Supply Tests	66
Table 3.4: Summary of Foot Sensor Unit Test	67
Table 3.5: Summary of System Control Unit Tests.....	68
Table 5.1: Dimensions of Preliminary Design.....	76
Table 5.2: Dimensions of COTS modules	76
Table 5.3: Size comparison of Preliminary vs Integrated designs.....	77

LIST OF FIGURES

Figure 1.1: (a) ReWalk Personal (ReWalk) front [22], (b) ReWalk Personal rear [22], (c) The Indego (Parker Hannifin) [23], (d) Ekso GT (Ekso Bionics) [24].....	8
Figure 1.2: Sit to Stand and Stepping in a lower body exoskeleton (from Ekso Bionics and [25])	9
Figure 1.3:a) Manual control of a lower limb orthotic, such as the wristwatch-like controller for the ReWalk (adapted from [28], and b) Automatic control of a robotic orthosis using body tilt to sense walking intention.....	10
Figure 1.4: The Gait Cycle (adapted from [37]).....	12
Figure 1.5: Leg geometry and reference angles for hip, knee, ankle [12]	13
Figure 1.6: Sagittal joint angles for Hip, Knee and Ankle. Red line: unperturbed. Blue line: perturbed. The shaded boundary is 3σ . [39]	14
Figure 1.7: Sampling of an arbitrary curve. The position (angle) of the corresponding joint has been normalized to 8-bit resolution (0 to 255).....	16
Figure 1.8: Illustration of PWM control of servomotor. The actuator has a 180° range of motion. Adapted from [48].....	17
Figure 2.1: The ARKE Generation 2.0 Exoskeleton [49].....	20
Figure 2.2: ARKE Simplified State Machine	21
Figure 2.3: Flowchart showing typical therapy session with device.	23
Figure 2.4: Walking Interface on Control Tablet [49].....	24
Figure 2.5: Top view of Preliminary logic board	25
Figure 2.6: Preliminary logic board in-situ with additional hardware components	25
Figure 2.7: Block diagram of exoskeleton system with Preliminary logic board.....	26
Figure 2.8: Power architecture of Integrated Design	38
Figure 2.9: Schematic Design of PPSU	42
Figure 2.10: Schematic of 12V Buck Converter in Integrated Design	43
Figure 2.11: Efficiency vs. Load Current and V_{in} curves for LM5010 regulator (adapted from [66]).....	43
Figure 2.12: JTAG port on Tiva C-Series Launchpad (adapted from [52])	47
Figure 2.13: JTAG Connection to PCB	49
Figure 2.14: System Block Diagram of Integrated Design.....	50

Figure 2.15: Block diagram of system with Integrated Design.	51
Figure 2.16: (a) top left: 2D layout of Microcontroller; (b) example of 3D model of part provided in Altium Vault; (c) examples of 3d models of parts provided by part vendor, (d) example of simple self-modeled part.....	52
Figure 2.17: 3D Isometric view of Integrated Design showing components and system interfaces	53
Figure 3.1 a) Top side and b) Bottom side of the bare board.	58
Figure 3.2 a) Various solder bridges are present across IC legs after reflow, b) A connector pulled askew during reflow.....	61
Figure 3.3 a) Assembled top side of PCB, b) Assembled bottom side of PCB, c) Close-up of IMU	62
Figure 3.4: Initial programming of the microcontroller. The microcontroller is loaded with the blink program. The LED on the lower left of the board is illuminated and flashes with the adjacent LED.	64
Figure 3.5: Reworked Buck Converter	65
Figure 3.6: Output of 12V0 buck converter.....	65
Figure 3.7 Testing the foot sensors. The left and right LEDs on the board illuminate when their respective foot sensor is occluded. a) Both sensors open, b) Left sensor occluded, c) Right sensor occluded, d) Both sensors occluded.....	67
Figure 3.8: Integrated Design advertising over Bluetooth.....	69
Figure 4.1: Workflow for collecting and processing walking session data	72
Figure 5.1: Joint angles and velocities of ARKE system using Preliminary Logic Board.....	74
Figure 5.2: Joint angles and velocities of ARKE system using Integrated Logic Board.....	75
Figure 6.1: Addition of reworked RC network to PCB.	79

LIST OF APPENDICES

APPENDIX A: PCB DRC RESULTS AND STACKUP.....	83
A.1 PCB Stackup.....	84
APPENDIX B: IR REFLOW OVEN	85
APPENDIX C: SCHEMATICS.....	86

1 INTRODUCTION

Robotics are considered as a new modality for treating disability [1,2]. When an individual's brain or central nervous system (CNS) is affected by injury or pathology (e.g. stroke), he/she may suffer from varying degrees of motor impairment. The resulting long-term effects of motor impairment, which include atrophy, denervation and cardiovascular disease [3-5], are still of great concern to affected individuals and their families. For example, the life expectancy of persons with spinal cord injury (SCI) remains significantly lower than the life expectancies of healthy individuals. Data, adapted from the US National Spinal Cord Injury Statistical Center [6], and listed in Table 1.1, indicate that on average persons with paraplegia live between 10 to 15 years less than healthy individuals.

Age at Injury	No SCI	Persons surviving the first 24 hours			Persons surviving at least 1 yr. post injury		
		AIS-D	Paraplegic	Low Tetra (C5-C8)	AIS-D	Para	Low Tetra (C5-C8)
20	59.5	52.6	45.1	40.0	52.9	45.5	40.7
40	40.6	34.2	27.7	23.5	34.5	28.1	24.1
60	23.1	17.9	13.1	10.3	18.2	13.4	10.6

Table 1.1: Life expectancies of persons with SCI [6]

The goal of robotic therapy, then, is to place the individual in a device which shares the movement and forces of healthy ("pathology-free") individuals and utilizes their neuroplasticity [7,8] to retrain their motor skills, while promoting innervation and redevelopment of muscle and bone density [9]. Through this training, it is hoped that these impairments can be corrected or mitigated.

There is a large range of new possibilities for rehabilitative robotics, including arms [8], [10] and legs. Legged machines have greatly evolved since the hopping machines of Raibert [11] in 1985. The advent of cheap and abundant computing as the result of Moore's law has allowed for a generational leap in the complexity of robots. Modern embedded systems have made computationally demanding applications possible in small, portable and inexpensive forms. Wearable mobile machines, known as exoskeletons, are an important innovation emerging from the flexibility and performance of such modern systems.

Exoskeletons can be generally described as systems consisting of powered joints and linkages enveloping the user, and can be divided into two main categories: 1) exoskeletons for performance augmentation, such as in [12-15], which increase the strength and endurance of the wearer with general use in civilian and military applications, and 2) exoskeletons used in the medical sector for rehabilitative purposes, such as in [16-18]. The second group can be further divided into partial-assist devices, which, like augmentative devices amplify the residual strength, and full-assist devices which completely control the wearer's movement. These rehabilitative devices, also known as orthoses, would be used to restore the walking ability lost due to disease or trauma such as SCI. Exoskeletons can also be classified into two groups: full and partial-body orthoses.

Partial body orthoses for lower limbs are presently a highly active field of research that is also experiencing growing public visibility. For instance, the 2014 FIFA World Cup in Brazil began with a kick by Juliano Pinto, a 29-year-old paraplegic, that was accomplished with the help of a full body exoskeleton and a brain-computer interface made by Brain Products [19]. Several companies are actively developing medical exoskeletons, including the Ryerson University-based Bionik Laboratories, Ekso Bionics, ReWalk, Parker, and Cyberdyne.

The design of medical exoskeletons poses numerous engineering challenges including the flexibility of the device to move and accommodate different user geometries, power control, fail-safe operation, and preventing joint fouling or other user injury. On the consumer side, these challenges are offset by the improved prognosis that they provide compared to the traditional wheelchair.

1.1 MOTIVATION

The existing lower body exoskeletons are large and cumbersome for users. This research aims to develop a miniaturized hardware platform using commercial electronics which will reduce the size of these devices, increasing their portability, range and therefore autonomy of their users. In addition, the design seeks to add modularity and extensibility to offset the high costs and risks associated with the development components for medical devices. Generally, the healthcare industry remains conservative due to liability. By enabling rapid design cycles without sacrificing performance, smaller and more capable orthoses will come to the market hopefully in the near future.

1.2 OBJECTIVES

The main objective of this work is to develop an extensible fully-assistive lower-body exoskeleton controller which coordinates the top-level control and interfacing tasks for the exoskeleton. The following stages were considered towards that goal:

1. Research and analyze the existing approaches to hardware design of robotic exoskeletons, their demands and constraints.
2. Develop and install prototype hardware platform into an existing exoskeleton system.
3. Demonstrate that the design i) is functional, ii) meets or exceeds the performance of an existing system through the collection and analysis of device performance data, and iii) reduces the size of an existing platform.
4. Identify possible improvements of the proposed hardware platform through testing.

1.3 AUTHOR'S CONTRIBUTION

The following contributions were made towards the main objective:

1. Performed an in-depth literature review of the existing medical lower body exoskeletons, PCB layout techniques and embedded design principles.
2. Collaborated with the ARKE team at Bionik Laboratories to develop hardware for prototype exoskeleton platform used for baseline performance; verified and validated design, then deployed controller in four ARKE systems for medical trials at rehabilitation centres in Ottawa and Montreal.
3. Clinical and engineering feedback was gathered over eight months of medical trials to revise the design, incorporating additional functionality and increasing the resilience.
4. Developed, fabricated and tested revised platform design in ARKE system.
5. Gathered performance data, performed analysis on results in MATLAB and translated observations into suggested features for future revisions.

1.4 THESIS LAYOUT

The following chapters are organized as follows:

- In Chapter 2, a detailed overview of the existing exoskeleton and how it works is provided. A preliminary design used for the command and data handling subsystem of the device is presented as the baseline for performance. The existing controller was analyzed for its shortcomings to improve upon the design. The improved design is presented, with focus placed on improving resilience and extensibility of the platform.
- Chapter 3 presents the validation process for assembling a unit of the improved design. A unit is assembled and tested prior to insertion into the system for performance evaluation.
- Chapter 4 presents the experiment used for gathering performance data, as well as the methodology behind data collection and post-processing.
- Chapter 5 contrasts the results of the Preliminary design with the Integrated, and a size analysis is performed on the two designs.
- Chapter 6 presents the conclusions of the thesis, and proposes improvements to the design, recommendations and future works.

1.5 BACKGROUND

The following background is provided to give insight into the current state-of-the-art design of lower body orthoses and the operational theory, including the emulation of walking kinematics. Several exoskeletons that are currently used in clinical settings are discussed in Section 1.5.1.

1.5.1 State of the art

In Canada and the United States, medical devices such as these orthoses are subject to regulatory compliance before authorization for sale. The governing bodies for these countries are Health Canada and the FDA, respectively. Examples of Health Canada or FDA approved lower body orthoses are the ReWalk Personal (ReWalk Robotics, shown in Figure 1.1a and b) [16], Indego (Parker Hannifin, Figure 1.1c) [20] and Ekso GT (Ekso Bionics, Figure 1.1d) [21]. These orthoses are intended for clinical use, and, in the case of the ReWalk and Indego, also for home use.

Each orthotic follows a common mechanical design, consisting of a fitted metal frame with a computerized control system worn on the user's trunk. Fabric padding is provided for user's comfort and to minimize skin abrasion.

Similarly, each orthotic uses a symmetrical four-axis arrangement to implement walking trajectories along the sagittal plane. Whereas the hip is a spherical joint with a complicated six degrees of freedom (DOF) range of movement, these devices approximate the motion using single revolutionary joints due to the difficulty of reproducing this range of motion robotically. The loss of these DOF is not necessary to approximate walking.



(a)



(b)



(c)



(d)

Figure 1.1: (a) ReWalk Personal (ReWalk) front [22], (b) ReWalk Personal rear [22], (c) The Indego (Parker Hannifin) [23], (d) Ekso GT (Ekso Bionics) [24].

These orthoses perform sit-to-stand and stand-to-sit motions which allow users with varying levels of hemiparesis or paralysis to stand and walk over level ground. Some orthoses, such as the ReWalk, can also navigate stairs. Figure 1.2 shows a typical sit-to-stand motion. It should be noted that the user is reliant on a pair of crutches for maintaining balance and navigating while inside the orthotic. These orthoses, therefore, are not intended for individuals with upper extremity disability.



Figure 1.2: Sit to Stand and Stepping in a lower body exoskeleton (from Ekso Bionics and [25])

To allow for free roaming in clinical and neighborhood settings, these orthoses are powered by rechargeable batteries which allow for several hours of use.

Two means of user input are generally provided by each orthotic. The first is control from an external apparatus, such as a wireless controller (ReWalk, shown in Figure 1.3a), tethered remote (Ekso GT), or smartphone application (Indego). The second is via the use of onboard microelectromechanical (MEMS) sensors which detect angular and translational displacement and forces of the orthotic. Rueterbories et al. in a study of various orthoses conclude that the most common types of sensors found are accelerometers typically in combination with gyroscopes, with little criticality as to the positioning of the sensors in the device [26]. These sensors determine user

intent via means ranging from binary thresholding of these sensor values to complex multi-sensor algorithms. An example of accelerometry being used to determine walking intention is shown in Figure 1.3b. By measuring tilt, an orthotic can detect the user's center of gravity (COG) shifting onto the stance leg, which, in healthy gait, precedes the motion of the swing leg. This can be used to trigger the leg motion of the orthotic. Other orthoses, such as the Cyberdyne HAL, use ground forces to detect user intention [27]. Many other methods exist, however the choice of sensor should emphasize reliability, minimizing components and size, and user acceptance [26].

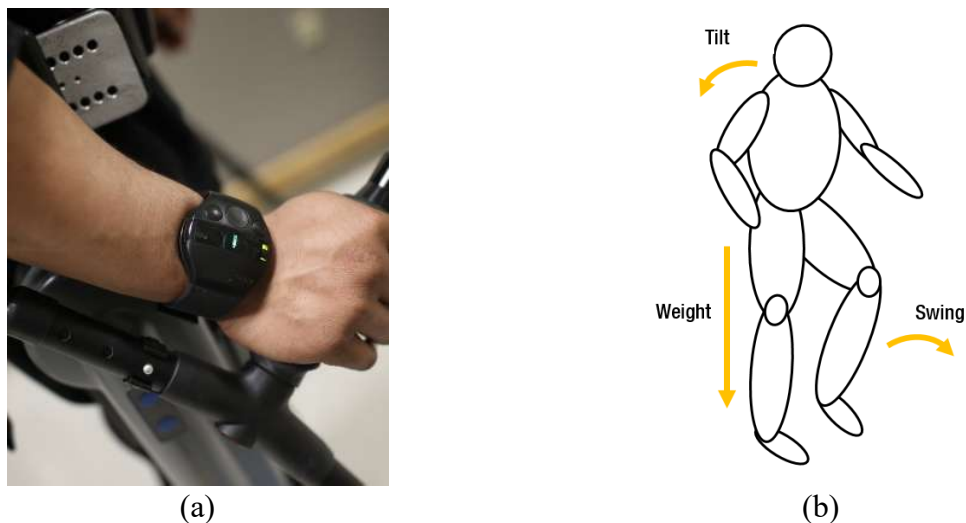


Figure 1.3: a) Manual control of a lower limb orthotic, such as the wristwatch-like controller for the ReWalk (adapted from [28]), and b) Automatic control of a robotic orthosis using body tilt to sense walking intention

The user characteristics and weights for the ReWalk, Ekso GT and Indego are listed in Table 1.2. These orthoses are designed to suit most of the population, either by being adjustable (such as for shared devices in clinical settings) or built personalized to each user.

Parameter	ReWalk	Ekso GT	Indego
User Height Range	5'3" (160cm) - 6'3" (190cm)	5'2" (157cm) - 6'2" (188cm)	5'1 (155cm) - 6'3 (191cm)
User Weight Range	Up to 220lb (100kg).	Up to 220lb (100kg).	Up to 250lbs (113kg)
Device Weight	Appx. 50lb (23kg)	Appx. 50lbs (23kg)	Appx. 26lb (12kg)
SCI Level:	T4 or lower	C7 or lower	C5 or lower

Table 1.2: Comparison of FDA approved lower body exoskeletons

The approximate cost of these orthoses are \$100,000USD each with an expected lifespan of 5 years [16].

1.5.2 Efficacy of Robotic Orthoses

The therapeutic benefits of bionic rehabilitation are presently the subject of intense study. Arazpour et al. [29] have summarized the medical studies on the efficacy of orthoses and generally found improved gait pattern and walking speed and reduced energy consumption. This is concurred by Benson et al. [30]. Kressler et al. [31] demonstrate reduced pain intensity with orthoses. Murtagh [16] found that lower body robotic orthoses are generally well tolerated with no serious adverse events reported for the devices.

1.5.3 Gait Cycle and Walking

Walking involves the intricate coordination of different muscles and joints coupled with sensory feedback used by the nervous system to correct disturbances or deviations from intended movement [32]. Walking, from a neurology perspective, consists of i) voluntary activation of the somatic nervous system with the intent to walk, ii) activation of the central nervous system and propagation of signals to muscles in the extremities, iii) muscle contraction, and iv) generation and regulation of muscle forces and joint torques [32,33].

A person's manner of walking is known as gait. The cyclic process of upright body locomotion is known as the gait cycle [34]. Biomechanically, pathology-free gait consists of bilaterally symmetrical swing and stance phases occupying 40% and 60% of each gait cycle, respectively [15]. These phases overlap with the swing phase for one leg starting during the stance phase of the other. A gait cycle can also be further broken down into the following phases: Heel Strike,

Foot Flat, Mid-Stance, Push-Off (also referred to as Heel-Off), Toe-Off and Mid-Swing [34–36].

Figure 1.4 illustrates a gait cycle.

In addition, a gait cycle can also be divided into single support (when only one foot is in contact with the floor) and double support (when both feet are in contact with the floor) phases.

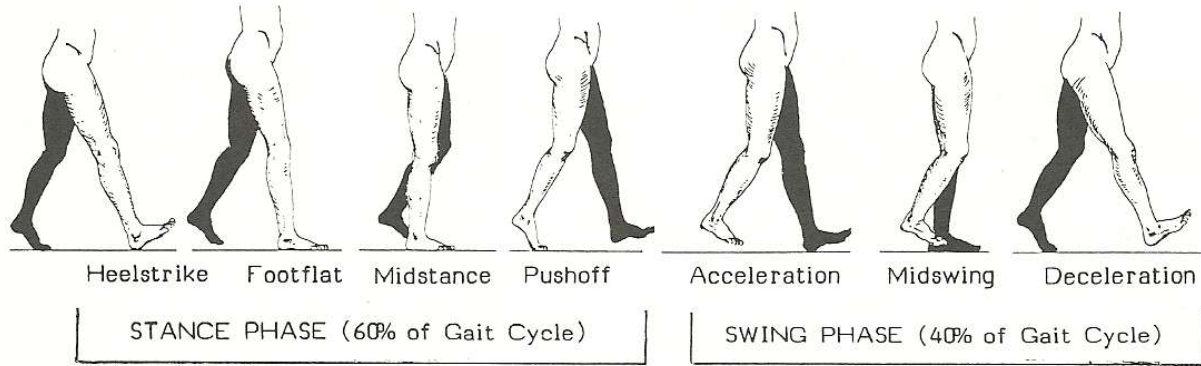


Figure 1.4: The Gait Cycle (adapted from [37])

1.5.4 Forward Kinematics and Trajectory

The trajectory of the lower body during the gait cycle has been extensively modeled by researchers like Hogan [38]. These models are used as a reference for approximation of human walking by lower limb orthoses.

First consider the lower body in the sagittal plane. Without loss of generality, consider the joint angles of one leg since the body is bilaterally symmetric. Figure 1.5 shows the geometry of the hip, knee and ankle. Zoss et al. [12] and Moore et al. [39] use the convention of defining the nominal (zero) angles for the hip (θ_{Hip}), knee (θ_{Knee}) and ankle (θ_{Ankle}) to be such that the vectors from the shoulder to the hip, the hip to knee, knee to heel, and heel to toe be collinear.

1 INTRODUCTION

Robotics are considered as a new modality for treating disability [1,2]. When an individual's brain or central nervous system (CNS) is affected by injury or pathology (e.g. stroke), he/she may suffer from varying degrees of motor impairment. The resulting long-term effects of motor impairment, which include atrophy, denervation and cardiovascular disease [3-5], are still of great concern to affected individuals and their families. For example, the life expectancy of persons with spinal cord injury (SCI) remains significantly lower than the life expectancies of healthy individuals. Data, adapted from the US National Spinal Cord Injury Statistical Center [6], and listed in Table 1.1, indicate that on average persons with paraplegia live between 10 to 15 years less than healthy individuals.

Age at Injury	No SCI	Persons surviving the first 24 hours			Persons surviving at least 1 yr. post injury		
		AIS-D	Paraplegic	Low Tetra (C5-C8)	AIS-D	Para	Low Tetra (C5-C8)
20	59.5	52.6	45.1	40.0	52.9	45.5	40.7
40	40.6	34.2	27.7	23.5	34.5	28.1	24.1
60	23.1	17.9	13.1	10.3	18.2	13.4	10.6

Table 1.1: Life expectancies of persons with SCI [6]

The goal of robotic therapy, then, is to place the individual in a device which shares the movement and forces of healthy ("pathology-free") individuals and utilizes their neuroplasticity [7,8] to retrain their motor skills, while promoting innervation and redevelopment of muscle and bone density [9]. Through this training, it is hoped that these impairments can be corrected or mitigated.

There is a large range of new possibilities for rehabilitative robotics, including arms [8], [10] and legs. Legged machines have greatly evolved since the hopping machines of Raibert [11] in 1985. The advent of cheap and abundant computing as the result of Moore's law has allowed for a generational leap in the complexity of robots. Modern embedded systems have made computationally demanding applications possible in small, portable and inexpensive forms. Wearable mobile machines, known as exoskeletons, are an important innovation emerging from the flexibility and performance of such modern systems.

Exoskeletons can be generally described as systems consisting of powered joints and linkages enveloping the user, and can be divided into two main categories: 1) exoskeletons for performance augmentation, such as in [12-15], which increase the strength and endurance of the wearer with general use in civilian and military applications, and 2) exoskeletons used in the medical sector for rehabilitative purposes, such as in [16-18]. The second group can be further divided into partial-assist devices, which, like augmentative devices amplify the residual strength, and full-assist devices which completely control the wearer's movement. These rehabilitative devices, also known as orthoses, would be used to restore the walking ability lost due to disease or trauma such as SCI. Exoskeletons can also be classified into two groups: full and partial-body orthoses.

Partial body orthoses for lower limbs are presently a highly active field of research that is also experiencing growing public visibility. For instance, the 2014 FIFA World Cup in Brazil began with a kick by Juliano Pinto, a 29-year-old paraplegic, that was accomplished with the help of a full body exoskeleton and a brain-computer interface made by Brain Products [19]. Several companies are actively developing medical exoskeletons, including the Ryerson University-based Bionik Laboratories, Ekso Bionics, ReWalk, Parker, and Cyberdyne.

The design of medical exoskeletons poses numerous engineering challenges including the flexibility of the device to move and accommodate different user geometries, power control, fail-safe operation, and preventing joint fouling or other user injury. On the consumer side, these challenges are offset by the improved prognosis that they provide compared to the traditional wheelchair.

1.1 MOTIVATION

The existing lower body exoskeletons are large and cumbersome for users. This research aims to develop a miniaturized hardware platform using commercial electronics which will reduce the size of these devices, increasing their portability, range and therefore autonomy of their users. In addition, the design seeks to add modularity and extensibility to offset the high costs and risks associated with the development components for medical devices. Generally, the healthcare industry remains conservative due to liability. By enabling rapid design cycles without sacrificing performance, smaller and more capable orthoses will come to the market hopefully in the near future.

1.2 OBJECTIVES

The main objective of this work is to develop an extensible fully-assistive lower-body exoskeleton controller which coordinates the top-level control and interfacing tasks for the exoskeleton. The following stages were considered towards that goal:

1. Research and analyze the existing approaches to hardware design of robotic exoskeletons, their demands and constraints.
2. Develop and install prototype hardware platform into an existing exoskeleton system.
3. Demonstrate that the design i) is functional, ii) meets or exceeds the performance of an existing system through the collection and analysis of device performance data, and iii) reduces the size of an existing platform.
4. Identify possible improvements of the proposed hardware platform through testing.

1.3 AUTHOR'S CONTRIBUTION

The following contributions were made towards the main objective:

1. Performed an in-depth literature review of the existing medical lower body exoskeletons, PCB layout techniques and embedded design principles.
2. Collaborated with the ARKE team at Bionik Laboratories to develop hardware for prototype exoskeleton platform used for baseline performance; verified and validated design, then deployed controller in four ARKE systems for medical trials at rehabilitation centres in Ottawa and Montreal.
3. Clinical and engineering feedback was gathered over eight months of medical trials to revise the design, incorporating additional functionality and increasing the resilience.
4. Developed, fabricated and tested revised platform design in ARKE system.
5. Gathered performance data, performed analysis on results in MATLAB and translated observations into suggested features for future revisions.

1.4 THESIS LAYOUT

The following chapters are organized as follows:

- In Chapter 2, a detailed overview of the existing exoskeleton and how it works is provided. A preliminary design used for the command and data handling subsystem of the device is presented as the baseline for performance. The existing controller was analyzed for its shortcomings to improve upon the design. The improved design is presented, with focus placed on improving resilience and extensibility of the platform.
- Chapter 3 presents the validation process for assembling a unit of the improved design. A unit is assembled and tested prior to insertion into the system for performance evaluation.
- Chapter 4 presents the experiment used for gathering performance data, as well as the methodology behind data collection and post-processing.
- Chapter 5 contrasts the results of the Preliminary design with the Integrated, and a size analysis is performed on the two designs.
- Chapter 6 presents the conclusions of the thesis, and proposes improvements to the design, recommendations and future works.

1.5 BACKGROUND

The following background is provided to give insight into the current state-of-the-art design of lower body orthoses and the operational theory, including the emulation of walking kinematics. Several exoskeletons that are currently used in clinical settings are discussed in Section 1.5.1.

1.5.1 State of the art

In Canada and the United States, medical devices such as these orthoses are subject to regulatory compliance before authorization for sale. The governing bodies for these countries are Health Canada and the FDA, respectively. Examples of Health Canada or FDA approved lower body orthoses are the ReWalk Personal (ReWalk Robotics, shown in Figure 1.1a and b) [16], Indego (Parker Hannifin, Figure 1.1c) [20] and Ekso GT (Ekso Bionics, Figure 1.1d) [21]. These orthoses are intended for clinical use, and, in the case of the ReWalk and Indego, also for home use.

Each orthotic follows a common mechanical design, consisting of a fitted metal frame with a computerized control system worn on the user's trunk. Fabric padding is provided for user's comfort and to minimize skin abrasion.

Similarly, each orthotic uses a symmetrical four-axis arrangement to implement walking trajectories along the sagittal plane. Whereas the hip is a spherical joint with a complicated six degrees of freedom (DOF) range of movement, these devices approximate the motion using single revolutionary joints due to the difficulty of reproducing this range of motion robotically. The loss of these DOF is not necessary to approximate walking.



(a)



(b)



(c)



(d)

Figure 1.1: (a) ReWalk Personal (ReWalk) front [22], (b) ReWalk Personal rear [22], (c) The Indego (Parker Hannifin) [23], (d) Ekso GT (Ekso Bionics) [24].

These orthoses perform sit-to-stand and stand-to-sit motions which allow users with varying levels of hemiparesis or paralysis to stand and walk over level ground. Some orthoses, such as the ReWalk, can also navigate stairs. Figure 1.2 shows a typical sit-to-stand motion. It should be noted that the user is reliant on a pair of crutches for maintaining balance and navigating while inside the orthotic. These orthoses, therefore, are not intended for individuals with upper extremity disability.



Figure 1.2: Sit to Stand and Stepping in a lower body exoskeleton (from Ekso Bionics and [25])

To allow for free roaming in clinical and neighborhood settings, these orthoses are powered by rechargeable batteries which allow for several hours of use.

Two means of user input are generally provided by each orthotic. The first is control from an external apparatus, such as a wireless controller (ReWalk, shown in Figure 1.3a), tethered remote (Ekso GT), or smartphone application (Indego). The second is via the use of onboard microelectromechanical (MEMS) sensors which detect angular and translational displacement and forces of the orthotic. Rueterbories et al. in a study of various orthoses conclude that the most common types of sensors found are accelerometers typically in combination with gyroscopes, with little criticality as to the positioning of the sensors in the device [26]. These sensors determine user

intent via means ranging from binary thresholding of these sensor values to complex multi-sensor algorithms. An example of accelerometry being used to determine walking intention is shown in Figure 1.3b. By measuring tilt, an orthotic can detect the user's center of gravity (COG) shifting onto the stance leg, which, in healthy gait, precedes the motion of the swing leg. This can be used to trigger the leg motion of the orthotic. Other orthoses, such as the Cyberdyne HAL, use ground forces to detect user intention [27]. Many other methods exist, however the choice of sensor should emphasize reliability, minimizing components and size, and user acceptance [26].

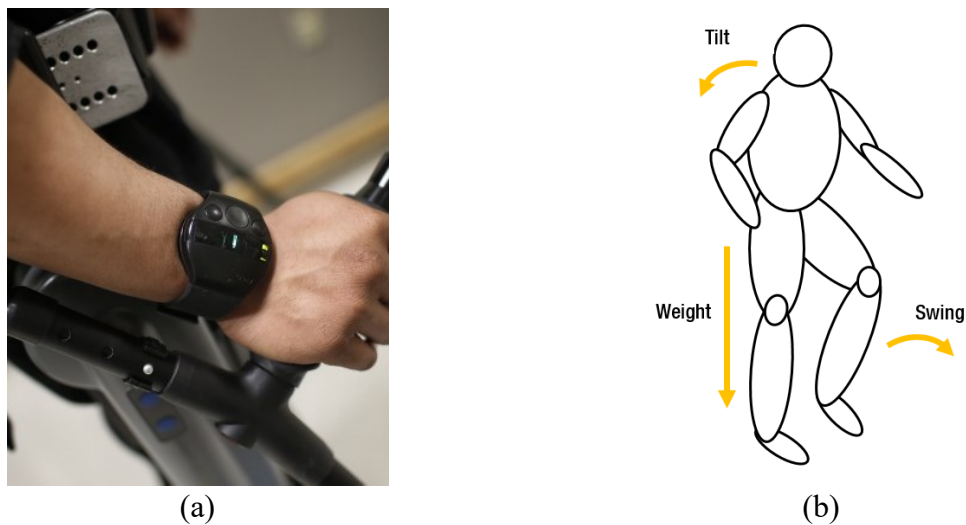


Figure 1.3: a) Manual control of a lower limb orthotic, such as the wristwatch-like controller for the ReWalk (adapted from [28]), and b) Automatic control of a robotic orthosis using body tilt to sense walking intention

The user characteristics and weights for the ReWalk, Ekso GT and Indego are listed in Table 1.2. These orthoses are designed to suit most of the population, either by being adjustable (such as for shared devices in clinical settings) or built personalized to each user.

Parameter	ReWalk	Ekso GT	Indego
User Height Range	5'3" (160cm) - 6'3" (190cm)	5'2" (157cm) - 6'2" (188cm)	5'1 (155cm) - 6'3 (191cm)
User Weight Range	Up to 220lb (100kg).	Up to 220lb (100kg).	Up to 250lbs (113kg)
Device Weight	Appx. 50lb (23kg)	Appx. 50lbs (23kg)	Appx. 26lb (12kg)
SCI Level:	T4 or lower	C7 or lower	C5 or lower

Table 1.2: Comparison of FDA approved lower body exoskeletons

The approximate cost of these orthoses are \$100,000USD each with an expected lifespan of 5 years [16].

1.5.2 Efficacy of Robotic Orthoses

The therapeutic benefits of bionic rehabilitation are presently the subject of intense study. Arazpour et al. [29] have summarized the medical studies on the efficacy of orthoses and generally found improved gait pattern and walking speed and reduced energy consumption. This is concurred by Benson et al. [30]. Kressler et al. [31] demonstrate reduced pain intensity with orthoses. Murtagh [16] found that lower body robotic orthoses are generally well tolerated with no serious adverse events reported for the devices.

1.5.3 Gait Cycle and Walking

Walking involves the intricate coordination of different muscles and joints coupled with sensory feedback used by the nervous system to correct disturbances or deviations from intended movement [32]. Walking, from a neurology perspective, consists of i) voluntary activation of the somatic nervous system with the intent to walk, ii) activation of the central nervous system and propagation of signals to muscles in the extremities, iii) muscle contraction, and iv) generation and regulation of muscle forces and joint torques [32,33].

A person's manner of walking is known as gait. The cyclic process of upright body locomotion is known as the gait cycle [34]. Biomechanically, pathology-free gait consists of bilaterally symmetrical swing and stance phases occupying 40% and 60% of each gait cycle, respectively [15]. These phases overlap with the swing phase for one leg starting during the stance phase of the other. A gait cycle can also be further broken down into the following phases: Heel Strike,

Foot Flat, Mid-Stance, Push-Off (also referred to as Heel-Off), Toe-Off and Mid-Swing [34–36].

Figure 1.4 illustrates a gait cycle.

In addition, a gait cycle can also be divided into single support (when only one foot is in contact with the floor) and double support (when both feet are in contact with the floor) phases.

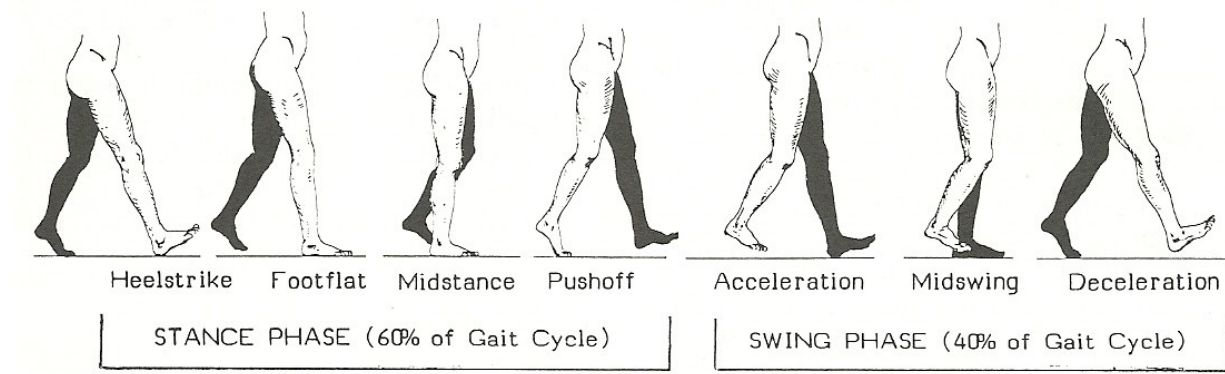


Figure 1.4: The Gait Cycle (adapted from [37])

1.5.4 Forward Kinematics and Trajectory

The trajectory of the lower body during the gait cycle has been extensively modeled by researchers like Hogan [38]. These models are used as a reference for approximation of human walking by lower limb orthoses.

First consider the lower body in the sagittal plane. Without loss of generality, consider the joint angles of one leg since the body is bilaterally symmetric. Figure 1.5 shows the geometry of the hip, knee and ankle. Zoss et al. [12] and Moore et al. [39] use the convention of defining the nominal (zero) angles for the hip (θ_{Hip}), knee (θ_{Knee}) and ankle (θ_{Ankle}) to be such that the vectors from the shoulder to the hip, the hip to knee, knee to heel, and heel to toe be collinear.

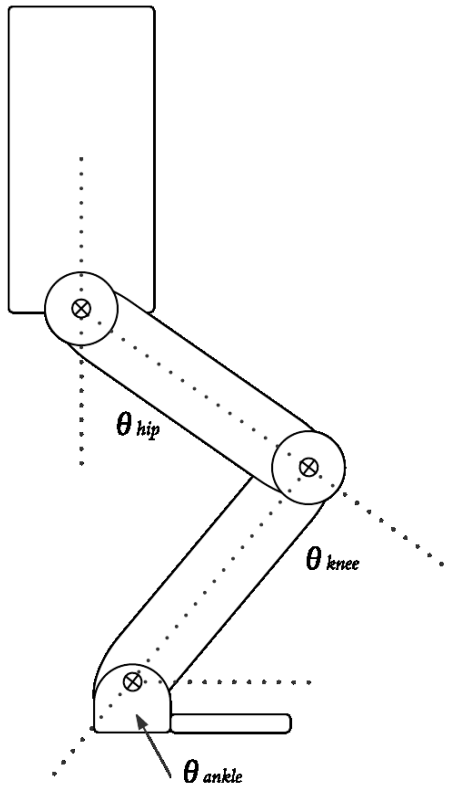


Figure 1.5: Leg geometry and reference angles for hip, knee, ankle [12]

Based on this convention, the corresponding joint angles for a typical leg over a pathology-free gait cycle in the sagittal plane are shown in Figure 1.6, from [39].

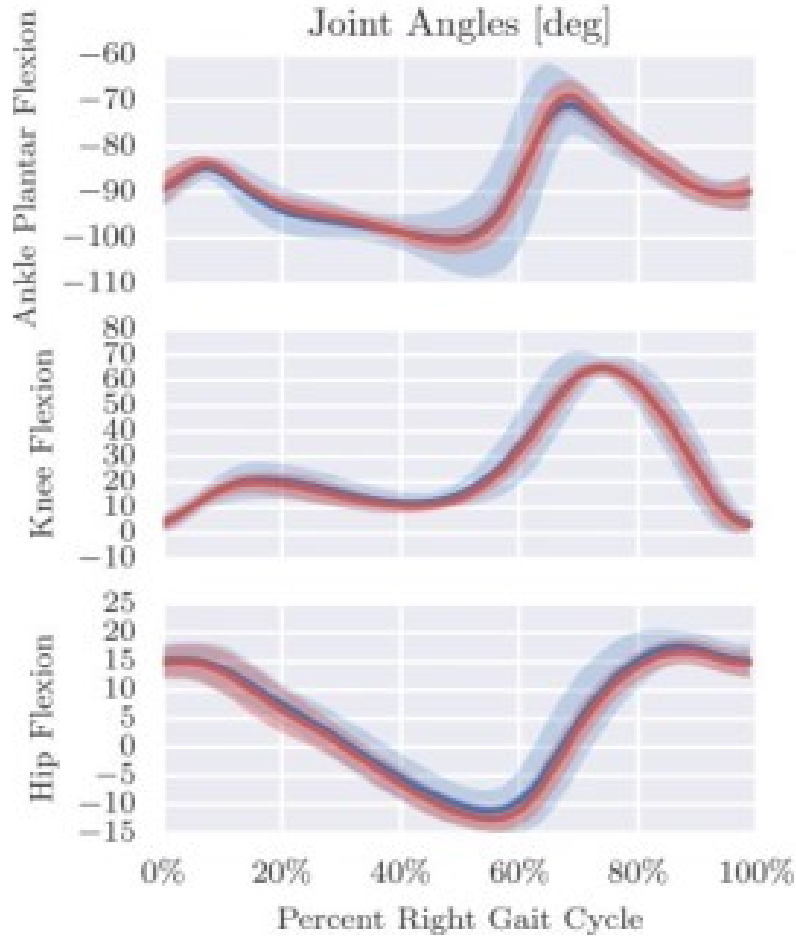


Figure 1.6: Sagittal joint angles for Hip, Knee and Ankle. Red line: unperturbed. Blue line: perturbed. The shaded boundary is 3σ . [39]

There are numerous methods for implementing the trajectories shown in Figure 1.6. One involves splines, numeric functions defined by piecewise polynomial functions, to generate a smooth trajectory [40]. This requires large computational overhead since only the parameters are stored and trajectory data are synthesized at runtime. However, this method has the benefit of being more flexible to online modification, such as to scale trajectories for different user proportionalities. A simpler albeit less flexible method is to store sample values in a lookup table (LUT) at the sampling frequency of the trajectory. This involves less computational overhead at the expense of reduced runtime flexibility (i.e., more difficult to modify), and greater memory consumption. However,

several robots such as in [41, 42] combine the lookup table approach with genetic algorithms to create evolutionary device behavior. In addition, memory usage can be mitigated by minimizing the number of samples required to store the trajectory through means such as linear interpolation.

Whether the trajectory data are computed or pre-calculated and stored, smooth motion is essential for the proper mobility of these orthoses. Slow control loops result in jittery motion, which would be unsuitable for the end user. One generally sought minimum control loop frequency for smooth actuator control is 1 kHz. This is used by Boston Dynamics' BigDog [43] robot and others, such as in [44, 45].

Figure 1.7 shows an example curve sampled at various points along the cycle. In the LUT approach, the samples shown would be stored in contiguous memory. In the spline approach, these would be calculated based on the polynomial coefficients and a time parameter. These samples are passed onto the servomotor controller as the desired position setpoint for the given instant in time [46]. The resolution as to which these samples are stored or calculated is chosen based on the range of movement and mechanical resolution of the actuator and feedback mechanism. In Figure 1.7, 8-bit resolution is shown, represented in hexadecimal. An unsigned 8-bit value can take on values ranging from 0 to 255. For an actuator with a 180 degree range of motion, this corresponds to $0.70^\circ/\text{LSB}$.

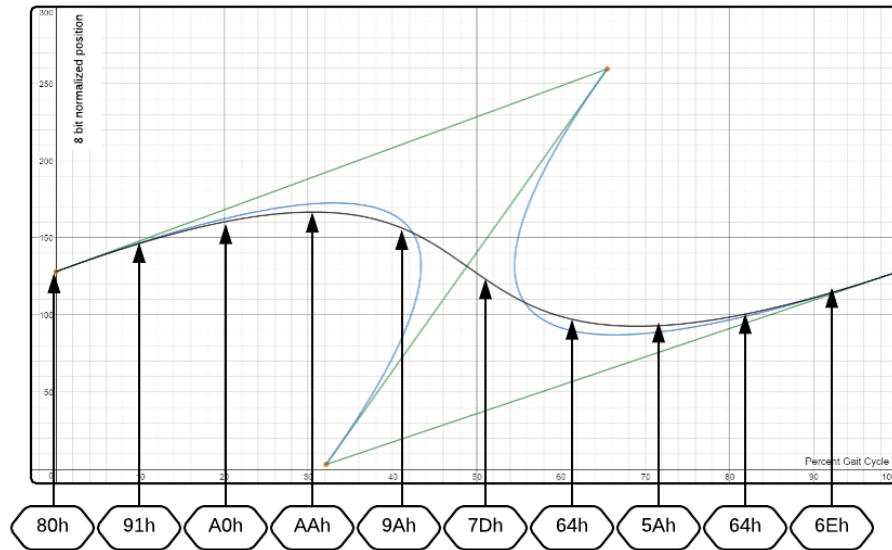


Figure 1.7: Sampling of an arbitrary curve. The position (angle) of the corresponding joint has been normalized to 8-bit resolution (0 to 255)

1.5.5 Motor Control

A servomotor is an actuator coupled with a feedback mechanism and controller which allows for precise control of position or velocity [47]. While servomotors may be AC or DC powered depending on the motor type, brushless DC motors (BLDCs) are popular in robotics since their construction lends themselves to fine positional control, and they require less maintenance and have greater efficiency than their brushed counterparts.

One common interface for positional control off-the-shelf servomotor drives is pulse-width modulation (PWM). In this configuration, the position of the actuator is mapped to the duty cycle of a control signal, as shown in Figure 1.8. The trajectory is executed by varying the duty cycle over time. For an 8-bit resolution PWM signal (such as the one used in Figure 1.7) the value '0' maps to a duty cycle of 0%, '128' ('80' hexadecimal) maps to a duty cycle of 50%, and '255' ('FF' hexadecimal) maps to a duty cycle of 100%.

PWM modules are common peripherals on modern microcontrollers, and these waveforms can be generated by loading a register with the desired positional value. Different interfaces such as RS-232, RS-485 and EtherCAT also exist where these set point values are transmitted in a digital frame to the servomotor drive. Unlike PWM, which is unidirectional, these interfaces allow for bidirectional communication. The benefit of bidirectional communication is that it enables multi-loop control and linear-parameter-varying systems (providing that the loop is sufficiently fast) since the servomotor data can now be read back by the main controller.

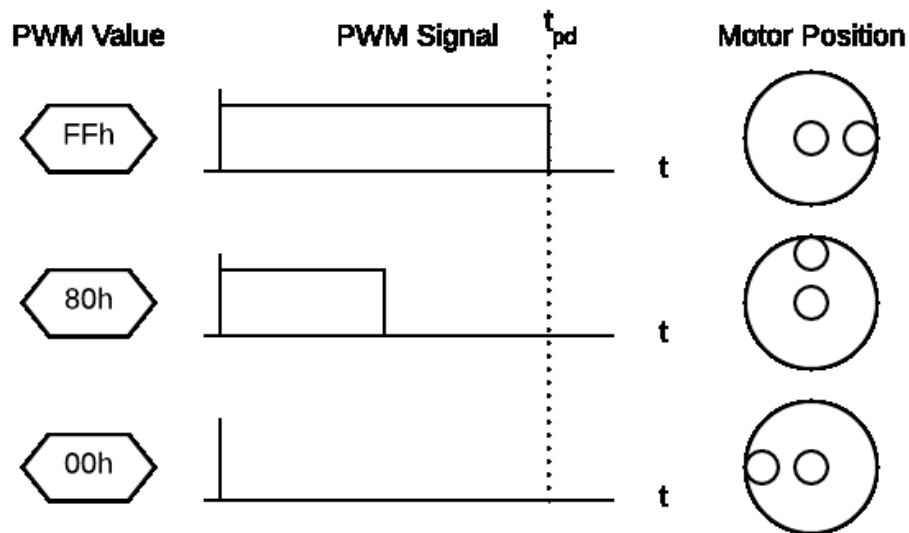


Figure 1.8: Illustration of PWM control of servomotor. The actuator has a 180° range of motion. Adapted from [48].

The controller for the servo provides the commutation sequence to move the motor to the desired position. Depending on the complexity of the drive, this may allow for PID routines.

2 PLATFORM DESIGN

2.1 INTRODUCTION

This chapter will discuss the theory and operation of a lower body exoskeleton, as well as the details of the designs of two hardware platforms used to run the main application firmware. The first design (the “Preliminary” design), is analyzed and used as a basis for the development of the second, successor platform, the “Integrated” design).

2.2 COLLABORATIVE WORK WITH BIONIK LABORATORIES

This research was part of a joint initiative conducted between Ryerson University and Bionik Laboratories Inc., a medical devices company based in Toronto, Canada and Ryerson DMZ alumnus. This collaboration granted access to a medical exoskeleton (The ARKE) as a hardware platform to test and verify research. In addition, this collaboration also included the deployment of ARKE units for medical study at The Ottawa Hospital Rehabilitation Centre (TOHRC) and the Institut de réadaptation Gingras-Lindsay-de-Montréal.

In addition to the two controller designs that were produced from this collaboration, many of the design constraints and requirements for the system and controller were developed in collaboration with the ARKE team. The Preliminary design was placed inside four ARKE units and deployed for medical study. Performance data and feedback were gathered from study participants and development team over the span of approximately 8 months.

2.3 THE ARKE

The ARKE Generation 2 (Figure 2.1) is a fully-assistive lower body exoskeleton in clinical research and development. The device is composed of adjustable padded linkages that cradle the user. The device has four motorized axes, two at the hips and knees, which actuate them along the sagittal plane. Two passive, spring loaded joints at the ankle provide flexion and extension and support the device which weighs approximately 34kg.

The system is powered by a removable lithium-ion battery pack, allowing untethered operation over environments with smooth terrain [49]. The device features adjustable trajectories based on user parameters such as leg length and hip width, walking and individual stepping modes, sit-to-stand, stand-to-sit, and patient or therapist triggered stepping.

The device is wirelessly commanded with a Windows-based tablet running proprietary ARKE control software, intended for use by a clinician or therapist. This tablet provides an API for data logging which is used for patient and engineering analysis.

Additional user interfaces include:

- MEMS sensors to measure the device attitude and forces which are used for the detection of walking intent
- A speaker for audio cues
- Foot sensors for ground contact detection

Brief overviews of the firmware and control tablet follow. This is provided for context to the hardware implementations described in this chapter.



Figure 2.1: The ARKE Generation 2.0 Exoskeleton [49]

2.3.1 Firmware Overview

A simplified version of the device state machine, shown in Figure 2.2, defines the high-level operation of the system.

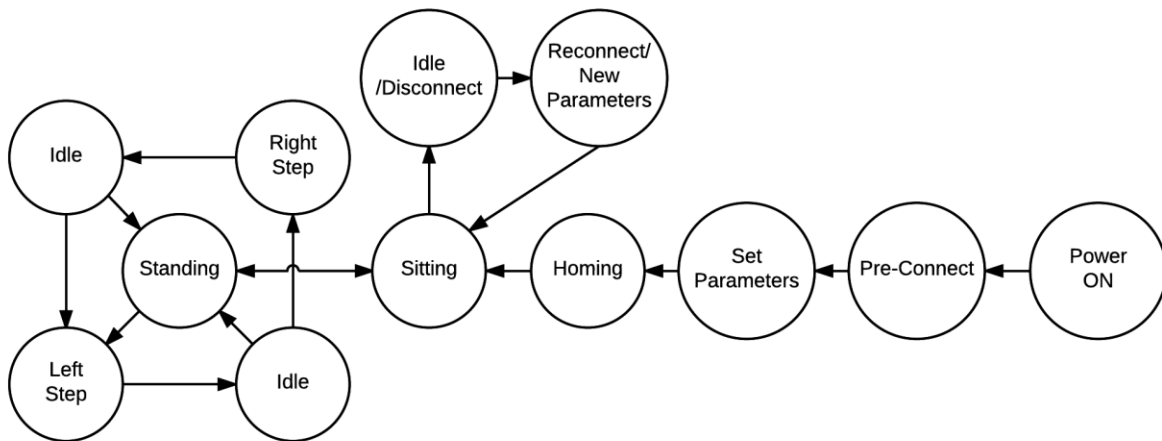


Figure 2.2: ARKE Simplified State Machine

The corresponding states are listed as follows:

- **Pre-Connect:** The device enters this state when first powered on or reset. The device sits idle waiting for the tablet to initiate a connection.
- **Set Parameters:** Upon successful handshake with the tablet, the device automatically downloads the device and session parameters.
- **Homing:** The device self-tests its actuators, aligns its axes, then moves to a seated position.
- **Sitting:** The device idles in a seated state. This is the position in which the user dons and doffs the device. The device stands when triggered by the operator (sit-to-stand motion).
- **Standing:** The device is upright. At this time, the operator may manually trigger stepping or enable patient control which uses the onboard inertial measurement unit (IMU) to

determine the walking intention of the user. The device then initiates a stride under the following conditions:

1. A command to step from the operator, in clinician control mode
2. The device tilt exceeds the minimum threshold set for the user, in patient control mode

Alternately, the device may be commanded by the operator to sit without initiating any walking sequence, such as to practice standing and sitting technique.

- **Left/Right Step:** The device executes a planned stepping trajectory for the corresponding leg. After completion of the stride, the system waits for user or operator input, then proceeds with the alternate leg. At the end of the exercise, a “stop” instruction brings the legs into alignment, and the device may then be seated or another walking session commenced. Note that the operator may switch modes arbitrarily; for example, the operator may begin a session by manually triggering steps, then hand off to the user for control, then take over if the user requires additional assistance.

Once the user has been seated at the end of the walking session, the operator finishes the session from the tablet which places the device into idle until a new session is initiated. At this time, the device may be powered off.

2.3.2 Application Overview

The operator interface and control of each ARKE device is performed via a Windows-based tablet running PatientProfile, a companion software for the device. PatientProfile configures the device and provides a touchscreen for operation. The sequence of a typical therapy session is shown in Figure 2.3. The operator first powers on the tablet, starts PatientProfile and retrieves the user profile. Settings, such as user dimensions, walking speed, and tilt sensitivity are loaded and

transferred to the device upon connection. Once the user dons the device, the operator commences the walking session by bringing the device and the patient to the standing position. In standing position, the operator is presented with the screen shown in Figure 2.4, allowing the choice of operating mode. The walking session then continues as described in the device state machine. In addition, PatientProfile tracks performance data for the device during the walking session and logs to a local database. The tablet API is further discussed in experimental data collection in Section 4.4.

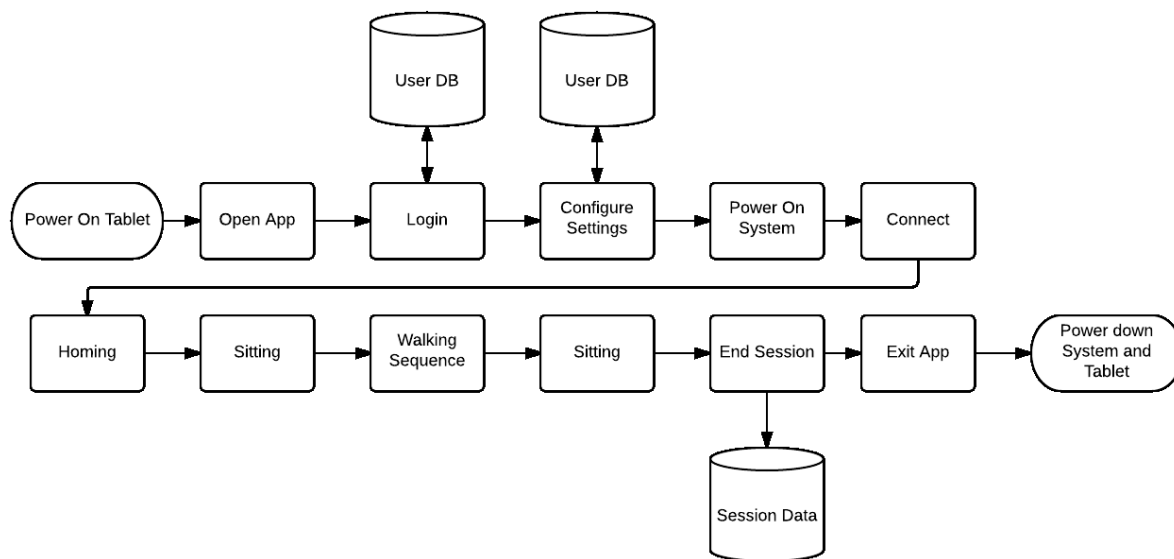


Figure 2.3: Flowchart showing typical therapy session with device.

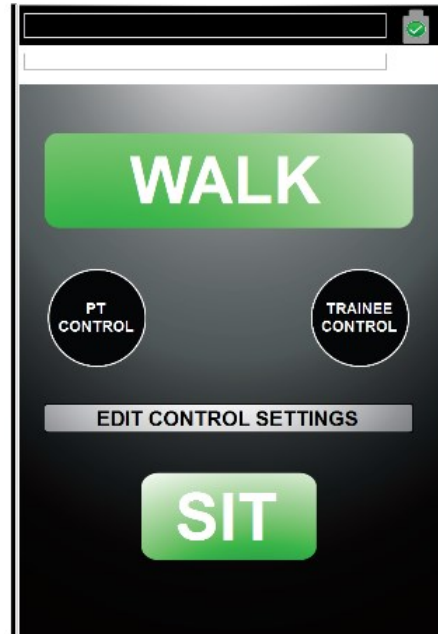


Figure 2.4: Walking Interface on Control Tablet [49]

2.4 PRELIMINARY DESIGN

The preliminary logic board design was co-developed in 2015 with the ARKE team and was used to determine baseline performance for a fully-assistive lower body exoskeleton.

Shown in Figure 2.5, the design used a custom interface board to modularly connect consumer-off-the-shelf (COTS) subsystems for the microcontroller, wireless, and IMU modules. These are detailed below. Logic power for the system was supplied by an external module adjacent to the logic board. This is shown alongside the fully assembled logic board in an early version of the system chassis in Figure 2.6.

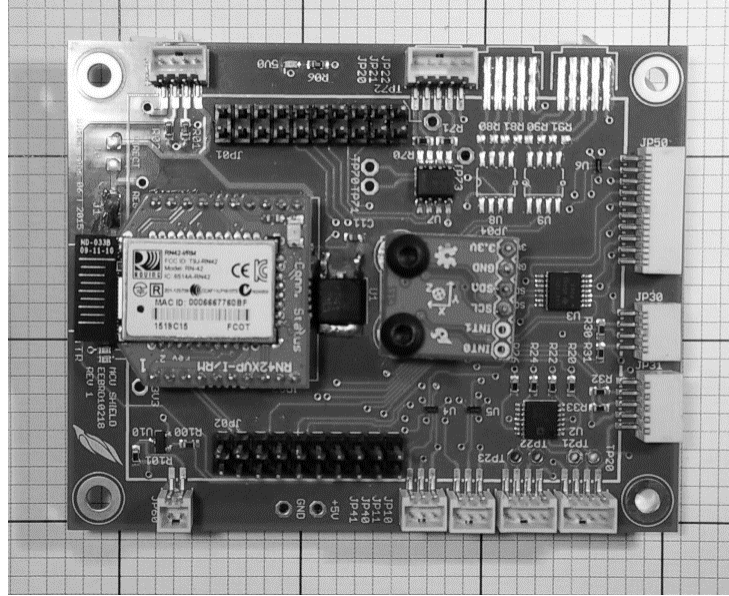


Figure 2.5: Top view of Preliminary logic board

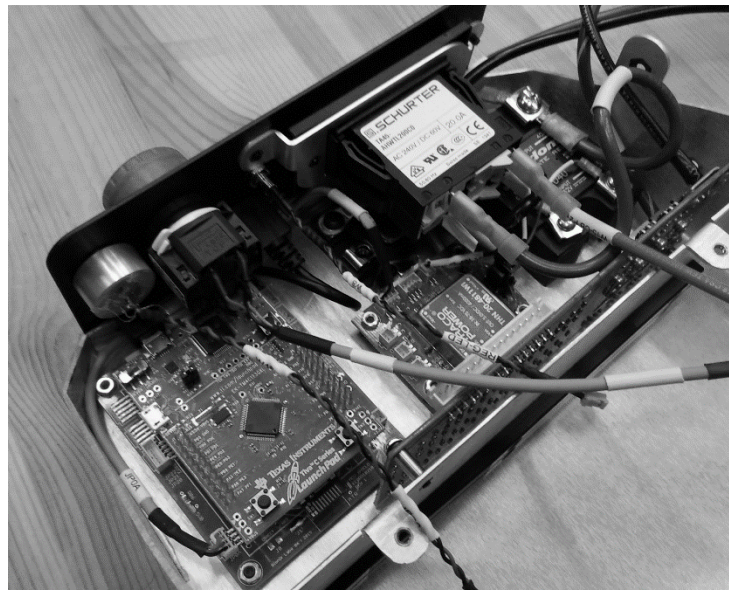


Figure 2.6: Preliminary logic board in-situ with additional hardware components

The logic board was responsible for the top-level command and data processing tasks for the system. Shown in a simplified system block diagram (Figure 2.7), the logic board interfaced with

discrete servomotor drives and system control peripherals, such as foot sensors for ground contact detection.

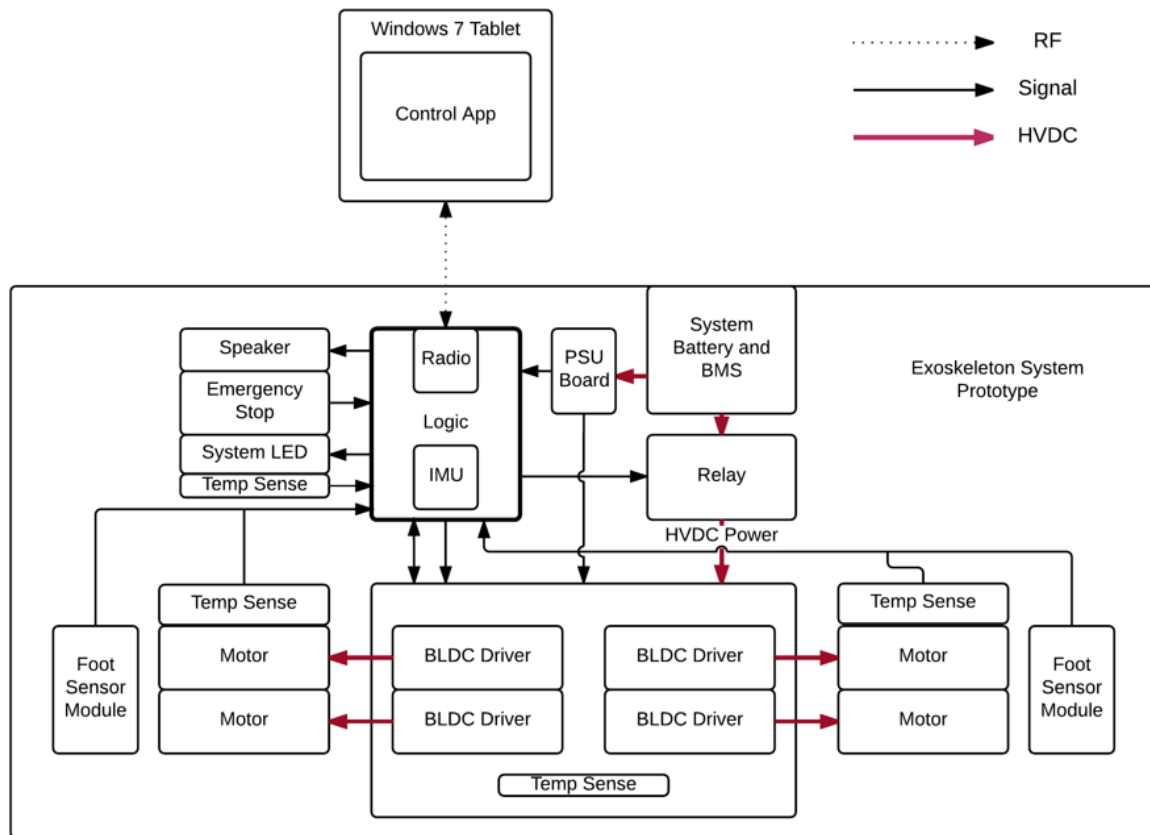


Figure 2.7: Block diagram of exoskeleton system with Preliminary logic board.

2.4.1 Microcontroller

The microcontroller on the logic board needed to perform the following tasks:

- Store and interpolate trajectory data for multiple user proportionalities
- Implement the device state machine
- Interface with local system control peripherals, such as speakers, temperature sensors and foot sensor modules

- Send and receive commands and data to and from the control tablet
- Send commands to and receive data from four brushless servomotor drives
- Read and filter IMU data

A COTS microcontroller module, the Texas Instruments Tiva C-series Launchpad, was chosen due to having sufficient GPIO, RAM and Flash to implement these interfaces as well as its adequate computational power (100DMIPS) [50] for these tasks and support for TI-RTOS [51]. The Tiva Launchpad is a general purpose evaluation kit featuring two headers for expansion modules (“Booster Packs”); a Tiva TM4C-series microcontroller using ARM Cortex M4 architecture, and an integrated USB JTAG emulator [52]. The decision to use the Launchpad system allowed for the flexibility to swap the microcontroller out with another Launchpad (such as the CC3200 or TM4C129x series microcontroller) if necessary, without having to redevelop the interfacing electronics.

2.4.2 Wireless Interface

The wireless interface of the system serves two functions: first, for receiving commands from the controller, and second, for streaming data. As shown in Figure 2.5, the design featured a 10x2 pin hardware socket commonly used by COTS RF modules such as XBee. In addition, many WiFi and Bluetooth modules use this socket. Bluetooth was chosen for point-to-point interoperability with standard end consumer hardware, such as tablets, phones and laptops, and the selected module was the Roving Networks RN42-XV [53]. The RN42XV module reliably supports virtual COM port operation over a UART interface at 115.2kBaud which was sufficient for the bandwidth requirements of the data. The advantage of these modules is that the communications overhead is offloaded from the main microcontroller, obviating the need for implementing a wireless stack.

2.4.3 IMU

Device attitude and acceleration were measured through a pair of MEMS sensors connected to the main microcontroller via I²C. These were:

- An InvenSense ITG-3200, a 3-axis gyroscope
- An Analog Devices ADXL345, a 13-bit resolution 3-axis accelerometer with programmable sensitivity ranges between $\pm 2g$ and $\pm 16g$

These devices were suitable due to their high resolution, low power consumption, and software support.

2.4.4 Servomotor Drives

The exoskeleton used four independent servomotor drive modules to drive the system's four custom non-backdrivable rotary actuators with built-in position encoders. These drives featured:

- Onboard PID control, allowing the control task to be offloaded from the main application host
- Voltage and current limiting
- In-depth status reporting (position, voltage, current, etc.) and
- RS232, RS-485 and PWM interfaces

These drives were mounted on a custom mounting card housed in the lower compartment of the system chassis. The logic board provided the trajectory information to the drivers over PWM and collected measurements over RS-485. RS-485 was chosen for data collection due to its multi-point addressing capability, necessitating only one transceiver for all four drivers, its industrially-robust

noise-rejecting differential, balanced twisted-pair design [54,55], its low cost, and its sufficient bandwidth to gather a snapshot of system data at a minimum of 50Hz. PWM was chosen for sending setpoint commands since each drive had a dedicated channel. Unlike RS-485, it involved no data frames or time-division multiplexing which would incur latency. This allowed the system to operate at the standard 1 kHz control loop required for smooth movement.

The PID parameters of these drives were tuned either in an external jig or in-situ via an RS-485 cable to a PC running the OEM configuration software for the drives. Overdamping was a requirement in order to maintain smooth operation and minimal vibration.

These drives were rated for peak current of 60A and were supplied with the nominal battery voltage, 48-60V DC. To protect the drives and actuators, the current was set to limit to 30 amps. These currents are possible during motor stall events such as a toe-strike or during sit-to-stand or stand-to-sit motions.

2.4.5 Summary of Preliminary Design

The Preliminary design performed generally well and its modular design successfully allowed rapid prototyping and development. By using COTS parts and interfaces, system parts could be easily and quickly serviced, swapped, and purchased with short lead-times. Human medical trials of four ARKE units with the Preliminary design commenced at the end of 2015. There were no failures of the prototype boards during the medical trials and, as of writing, the boards remain in-service.

2.5 SHORTCOMINGS OF PRELIMINARY DESIGN

The following observations were made about the Preliminary design.

2.5.1 Resilience

The Preliminary design relied on friction fit connections to hold the MCU and Bluetooth modules in position. Given that the typical operating environment of an exoskeleton exposes internal electrical components to harsh mechanical shock, it is expected that these connections fail over time. While this was not a problem in practice, the lifespan and durability of the board can be increased by eliminating these connections and other points of fatigue.

2.5.2 Extensibility

The Launchpad did not expose all available GPIO on the microcontroller. At any given time, only 34 of the 43 GPIO could be used [50, 56]. This limited the ability to expand the platform with new peripherals or functionality. The typical workaround for this was to conjoin several MCUs and/or mainboards together with wires, which created challenges for maintaining signal and power integrity across the PCBs, often manifesting as weak or unreliable connections. Placing the microcontroller directly into a new design would grant access to these GPIO, which would consist of a 26% increase in interfacing capability without changing the part or requiring a port of the firmware.

2.5.3 Signal Integrity

The stacked arrangement of PCBs in the Preliminary design created interconnected ground planes in 3D space. This resulted in multiple paths (loops) for current to flow and therefore added noise caused by electromagnetic induction. Recall the Maxwell-Faraday Equation [57]:

$$V = \oint_{dS} \mathbf{E} \cdot d\mathbf{l} = - \int_S \frac{\partial \mathbf{B}}{\partial t} \cdot d\mathbf{A} \quad (2.1)$$

which states that a time-variant magnetic field, such as those produced by external radiators, will produce a spatially-variant electric field, i.e. noise. The effect of the noise is proportional to the size of ground loops. Thus, it is preferable to minimize loop areas as much as possible in order to mitigate the effects of external radiators on the circuit. While digital circuitry is generally immune to this noise, analog circuitry remains susceptible, and is not desirable for high speed or resolution signals. This is concurred by [58] and [59]. The stacked design is therefore not preferable for signal integrity.

In addition, the stacked design adds challenges to controlling emissions to meet RF certification. The ability to add RF shielding is made less practical by the stacked design due to the additional height and volume of electronics.

Another consideration is that by separating the ground planes, impedance is added, resulting in larger supply and ground fluctuations with changes in current than a continuous i.e. low-impedance ground plane since

$$\frac{dV}{dt} = R \frac{dI}{dt} \quad (2.2)$$

for constant R .

2.5.4 Power Architecture

The Preliminary design used a 20W monolithic switching regulator providing a single trimmable output between 5.0 and 5.5V. This was set to 5.4V to meet the minimum voltage requirements for logic on the motor drivers and system logic board. This was regulated down to 5V with an LDO on the logic board, and a 3V3 LDO on the Launchpad. This regulator provided all logic power for the system.

During medical trials it was observed that the design was prone to resetting during high-torque events such as sit-to-stand, stand-to-sit and toe strikes, particularly for larger users. It has been shown [60] that the torque T for a 3 phase symmetrical brushless DC motor can be expressed as

$$T = \frac{2e_p i_p}{\omega_m} = |2K_t i_p| \quad (2.3)$$

where e_p , i_p , and ω_n are the back EMF of each phase, current of each phase and rotor speed, respectively. Since $T \propto i_p$, when T was maximum or changed rapidly, a high or rapidly changing current was observed on the primary DC bus as the motors attempted to maintain a mechanical steady state. This caused the primary DC bus voltage to spike or sag, which exceeded the line regulation capability of the 5.5V regulator which was supplied from the same bus. When the primary regulator output voltage fell below the minimum supply voltages of the downstream regulators and logic, the system lost state and reset.

Sudden resets pose risks of user injury since the user does not expect a sudden stop during movement. In addition, it may be difficult for the user to maintain his/her balance in the position the device has stopped at, and the system must return to a known good state with the user inside the device.

2.5.5 Design Conclusions for Preliminary Design

A new platform integrating the modular components onto one PCB would solve the issue of mechanical reliability, increase signal integrity, and provide an opportunity to redesign the power architecture, add new functionality and reduce assembly complexity and size of the platform. This work is undertaken in Section 2.6. The differences between the two design approaches are outlined in Table 2.1.

	Modular/COTS	Integrated	Remark
Mechanical Reliability	Added connectors for internal interfaces increase possible points of failure	Limited to external connectors only	Integrated preferred.
Power Integrity	Planes and regulators split across numerous PCBs. Inadequate line regulation with existing solution.	Contiguous power plane and ability to place regulators where desired.	Integrated preferred.
Signal Integrity	Vulnerable to noise from external radiators due to ground loops from stacked arrangement.	Ground loops minimized via singular PCB arrangement.	Integrated preferred.
EMI Compliance	Large signal loops also behave as external rad Stacked arrangement adds difficulty for RF shielding.	Easier to add in RF Shield on single-plane PCB.	Integrated preferred.
Size	Constrained by design of COTS parts.	Arbitrary. Can choose smaller footprints. Limited primarily by assembly complexity.	Integrated preferred.
Cost	Low upfront development costs. Large ongoing costs due to margins associated with intermediary parts.	Large upfront development costs and turnaround times. Better value is obtained through amortizing costs over large production runs.	COTS preferred for prototyping; Integrated preferred for production
Assembly	Requires component subassembly before system installation.	Drop-in ready.	Integrated preferred for production.
Extensibility	Launchpad only exposes 34 GPIO, high GPIO utilization means limited extensibility	All 43 GPIO made available; can use additional GPIO for expansion.	Integrated preferred.

Table 2.1 Comparison of Modular vs Integrated designs

2.6 THE INTEGRATED DESIGN

In this section the Integrated Design is introduced, starting with the requirements. The power and logic subsystems of the board are then presented and discussed in detail. The fabrication-ready design is shown. A full schematic representation of the Integrated design is attached in Appendix C.

2.6.1 Design Requirements

2.6.1.1 *System Compatibility*

The Integrated design must be mechanically and electrically compatible with the Preliminary design. This is necessary so that it can be fitted as a drop-in replacement for performance evaluation and comparison.

2.6.1.2 *Sizing and Placement of Components*

Due to the low production requirements of this design (3 units), hand-assembly needed to be feasible. Generally speaking, the costs of low-volume machine assembly are prohibitive. The components were therefore selected and laid out for easy hand-placement and reflow using the basic tools available in the lab: a microscope, an IR oven, a soldering iron and a hot air gun. This limited passive sizes to 0603 footprints or larger and restricted the use of BGAs, no-lead ICs or other fine-pitch components where possible. The two exceptions to this were the gyroscope and accelerometer which were unavailable in larger packages. Choosing hand-reworkable components also reduced the tolerance requirements for the PCB vendor, which in turn reduced the cost of the PCB.

Thermal reliefs were added to components connecting to large copper pours to ensure adequate reflow. This eliminated the main risk of having uneven copper pads, whereby during reflow one pad reflows before the other, causing the component to shift or lift off the board at an angle, in a process known as “tombstoning.”

Whereas the Preliminary design schematic and layout were performed in Eagle CAD 7.2, the schematic and layout of the integrated PCB were performed in Altium Designer 15. The decision to change the design tool was made based on the better ease-of-use and greater feature set of Altium, specifically the 3D modelling capabilities and online DRC. Altium’s 3D modelling capability allowed the design to be integrated into Solidworks MCAD to verify that the boards were mechanically compatible with the system chassis.

2.6.1.3 Requirements Tables

The requirements for the Integrated design are summarized in Tables 2.2 to 2.6.

Device Requirements:

ID	Requirement	Origin	Verification Method
DEV1	The device shall perform stand-to-sit, sit-to-stand and walking motions	Proposal	Design
DEV2	The device shall communicate wirelessly to the device controller	Proposal	Design
DEV3	The device shall record performance data and transmit them to device controller	Proposal	Design
DEV4	The device shall monitor attitude and acceleration	Proposal	Design
DEV5	The device shall monitor the temperature of heat generating components	Proposal	Design
DEV6	The device shall be extensible and reconfigurable	Proposal	Design

Table 2.2: Device-level requirements for Integrated Design

Mechanical Requirements:

ID	Requirement	Origin	Verification Method
MEC1	The design shall be mechanically compatible with the existing device	Proposal	Design
MEC2	The design shall be implemented on single PCB	Proposal	Design
MEC3	The design shall be robust	DEV1	Design, Test
MEC4	The design shall be designed to survive typical mechanical shocks	DEV1, MEC3	Design
MEC5	The design shall be low cost	Proposal	Design
MEC6	The design shall be small	Proposal	Design
MEC7	The design shall be capable of being hand assembled	MEC5	Design
MEC8	The design shall use 10 mil trace-space layout rule	MEC5, MEC7	Design

*Table 2.3: Mechanical Requirements for Integrated Design***Design Communication Requirements:**

ID	Requirement	Origin	Verification Method
COM1	The design shall communicate to host tablet using Bluetooth 2.1 + EDR	DEV2	Design, Test
COM2	The Bluetooth 2.1 module shall support serial port profile with virtual COM port at a minimum baudrate of 115,200bps	DEV2	Design, Test
COM3	The Bluetooth module shall be programmable in-situ	COM1, MEC2	Design, Test
COM4	The Bluetooth module shall be factory resettable with an external jumper	COM1, MEC3	Design, Test
COM5	The Bluetooth module shall advertise with a beacon when powered	COM1, DEV2	Design, Test
COM6	The Bluetooth module shall radiate RF energy away from the user as much as possible	Proposal	Design, Test
COM7	The design shall communicate to the servomotor drivers via single full-duplex RS-485	MEC1	Design, Test
COM8	The RS-485 link shall sustain a minimum baudrate of 921,600 bps	COM7	Design, Test
COM9	The design shall be capable of operating the device using local interface(s)	DEV6, MEC2,	Design, Test

Table 2.4: Communication Requirements for Integrated Design

Power Requirements:

ID	Requirement	Origin	Verification Method
PWR1	The board shall have a power supply	MEC2	Design
PWR2	The power supply shall power all internal system components	MEC2	Design
PWR3	The power supply shall accept the nominal battery voltage (40-70VDC)	MEC2, PWR1	Design
PWR4	The power supply shall output $3.3V \pm 100mV$	PWR2	Design, Test
PWR5	The power supply shall output $5.0V \pm 150mV$	PWR2	Design, Test
PWR6	The power supply shall output $12V \pm 2V$ with 400mA minimum ampacity	PWR2	Design, Test
PWR7	The power supply shall provide a field-trimmable power independent supply rail between 3.3V and 9V	DEV6	Design, Test

*Table 2.5: Power Requirements for Integrated Design***Processing Requirements:**

ID	Requirement	Origin	Verification Method
CPU1	The microcontroller shall have sufficient onboard memory to store trajectory data	DEV1	Design
CPU2	The microcontroller shall be compatible with and use the existing code-base	DEV1	Design
CPU3	The microcontroller shall have an interface for coprocessor or FPGA extension	DEV6	Design

Table 2.6: Processing Requirements for Integrated Design

2.6.2 Power Architecture

A new power architecture was developed for the Integrated design to resolve the regulator dropout issues observed in the Preliminary design. As per the requirements, the power subsystem would be integrated onto the PCB, providing regulated battery power for all system logic.

Increasing the voltage of switching regulator output was necessary to prevent the voltage ripple at the input from affecting downstream regulators. The choice of voltage was a compromise between compatibility, flexibility, footprint and heat. 12V was chosen to provide sufficient input margin, as well as for compatibility with the motor drivers and general industry. This was fed into cascaded regulators for supplying logic. An adjustable power supply unit, the PPSU, is provided and further described in 2.6.2.2. The block diagram of the power architecture is shown in Figure 2.8, detailing each component powered by each rail.

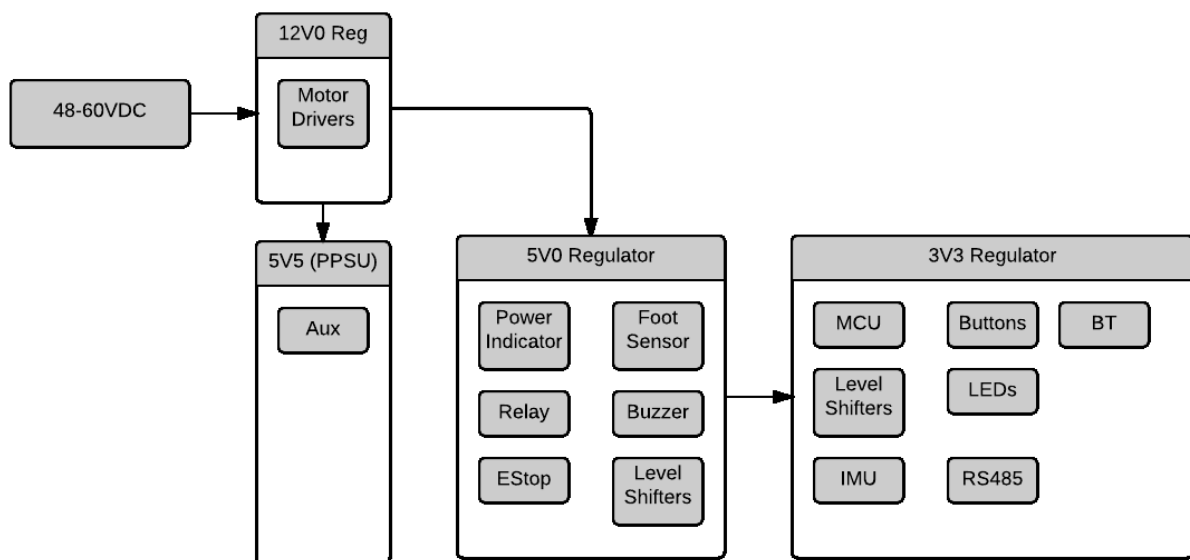


Figure 2.8: Power architecture of Integrated Design

To drive the design of regulators for each rail, the worst-case current draw and power figures were considered for each component. This is tabulated in the power budget for the system in Table 2.7.

In practice, the current consumption will be less due to the low duty cycle of some components; the average current consumption is expected to be 66-70% of the worst-case figure.

Peripheral	Rail	Current Draw	Power
Microcontroller	3.3V	58.7 mA	194 mW
Bluetooth	3.3V	50 mA	165 mW
IMU	3.3V	7 mA	23 mW
RS485 Transceiver	3.3V	20 mA	66 mW
LEDs and Buttons	3.3V	10 mA	33 mW
Miscellaneous	3.3V	20 mA	66 mW
3.3V Rail Total		165.7 mA	547 mW
3.3V LDO Power Dissipation			282 mW
Buzzer	5V	20 mA	100 mW
LED	5V	10 mA	50 mW
Miscellaneous	5V	20 mA	100 mW
5.0V Rail Total		215.7 mA	1.08W
5.0 LDO Power Dissipation			1.51 W
PPSU Rail Total	(Adjustable) 6V typ.	100mA	600mW
PPSU LDO Power Dissipation			600mW
Motor Drivers	12V	250mA	3W
12V Rail Total (Total System Current Consumption)		565.7 mA	6.79W
12V Converter Power Dissipation (Estimated 70% efficiency)			2.91W
Worst-Case Total Power Consumption:			9.70W

Table 2.7: Power Budget Table for Integrated logic board.

Two key architectures of DC-DC converters exist: switched and linear. Linear dropout regulators (LDOs) are attractive for being low-cost monolithic solutions for providing supply rails. However, their convenience comes at tradeoff with their relatively poor efficiency compared to switching regulators. Switched converters, in comparison, require a larger footprint, but provide better efficiency, typically in the range of 60-90%.

The heat dissipated by an LDO is the product of the output current times the difference between input and output voltages [61]:

$$P_D = (V_i - V_o) I_o \quad (2.4)$$

Equation 2.4 is used to calculate P_D for each the regulators listed in Table 2.7. Using Equation (2.4), it can be shown that:

$$\eta = \frac{P_o}{P_i} = \frac{P_o}{P_D + P_o} = \frac{V_o I_o}{(V_i - V_o) I_o + V_o I_o} = \frac{V_o I_o}{V_i I_o} = \frac{V_o}{V_i} \quad (2.5)$$

Thus, efficiency degrades proportional to the span of the input and output voltages. LDOs are therefore not suitable for designs where large input variances are required. For a 3.3V LDO supplied by 5V and a 5V LDO supplied by 12V, the theoretical efficiencies are 66% and 42%, respectively.

Given their relatively poor efficiencies, it is essential to consider the steady state regulator temperatures during design so that chip maximums are not exceeded. The temperature increase of the regulator ΔT_j corresponds to the product of the dissipated power and junction-ambient coefficient listed in the datasheet:

$$\Delta T_j = \theta_{ja} P_D \quad (2.6)$$

This is added to the ambient temperature to get the final junction temperature T_j . Heat can be mitigated at the design stage through the placement of copper pours on the PCB, by selecting larger chip footprints, and with the application of a heatsink. For V_i greater than 12V, the tradeoff between heat and size makes a 5V buck converter design preferable.

2.6.2.1 Board Linear Regulators

Three LDOs were selected for supplying the 3.3V, 5.0V and Programmable supply rails. These were the LM3940IMPX-3.3 [62], LM340MP-5.0 [63], and LM317AEMP [64], respectively. Using Table 2.1 and Equation 2.4, alongside parameters found in each of the components' respective datasheets, the thermal performance of each LDO is presented in Table 2.8, showing the selected LDOs are within safe operating limits under worst-case operation.

Rail	Part	P_D worst-case	θ_{ja} worst-case	T_j worst-case (at 25°C ambient)	Die Max Temperature
3.3V	LM3940IMPX-3.3	.282W	59.3°C/W	41.7°C	125°C
5.0V	LM340MP-5.0	1.51W	62.1°C/W	118.7°C	150°C
PPSU	LM317AEMP	.600W	59.6°C/W	60.7°C	125°C

Table 2.8: Heat analysis of LDO regulators of Integrated Design

2.6.2.2 Programmable Power Supply Unit (PPSU)

As part of the design's overall philosophy of extensibility, a programmable power supply was added for powering legacy or future peripherals. The schematic representation of this PPSU is shown in Figure 2.9. To leave the application of the power supply as open ended as possible, the PPSU can be configured for operation at voltages between 0 and 10V with the combination of two resistors. In addition to the voltage flexibility granted by choosing to power it from the 12V rail, this topology provides isolation from the 3.3V and 5V logic rails. Should faults or noise occur on this rail, they will not affect the main system logic.

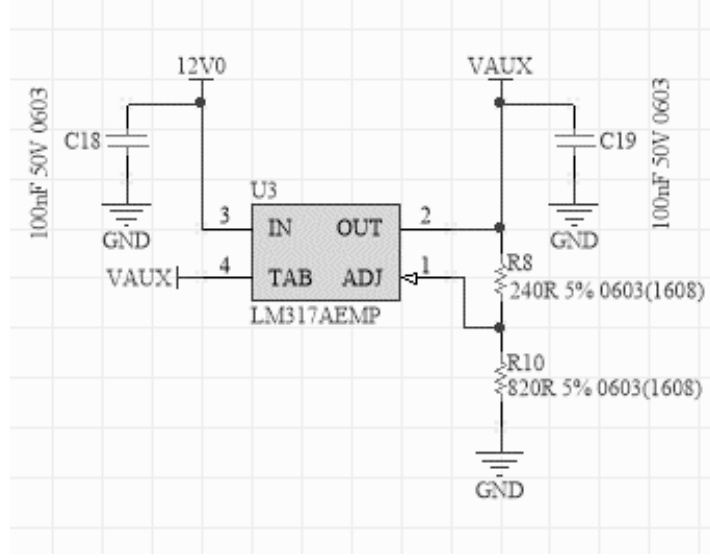


Figure 2.9: Schematic Design of PPSU

The voltage is set by the combination of R8 and R10 using the following relation:

$$V_{AUX} = 1.25 \left(1 + \frac{R_{10}}{R_8} \right) + I_{ADJ}(R_{10}) \quad (2.7)$$

Figure 2.9 shows the PPSU configured for a V_{AUX} of 5.5V.

2.6.2.3 Switching Regulator

Texas Instruments LM5010 [65] is a 1A non-synchronous buck regulator with a maximum input voltage of 75V. The benefits to this regulator include thermal protection, an integrated n-channel switch, undervoltage lockout, and constant switching frequency over load and line variation [66]. While monolithic modules like the one in the Preliminary design exist for 12V, this regulator is able to supply 12V at a substantially lower cost with greater flexibility for part substitution, and, despite requiring approximately 10 external components for operation, the regulator is realized in approximately the same footprint. The schematic representation of the 12V regulator for the Integrated design is shown in Figure 2.10.

The voltage of the regulator is defined by the combination of feedback resistors R7 and R9. The enable pin is connected high with resistor R6, however this may be disconnected and controlled by external hardware.

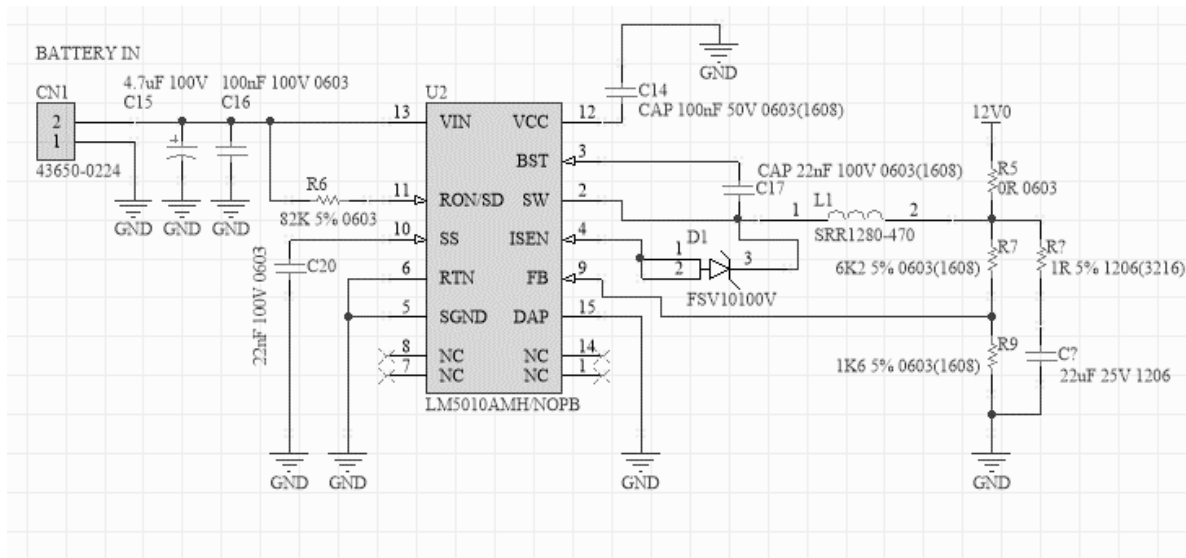


Figure 2.10: Schematic of 12V Buck Converter in Integrated Design

Figure 2.11 shows that the efficiency of the LM5010 regulator at the worst-case current load of approximately 600mA is approximately 75% with a 60V supply.

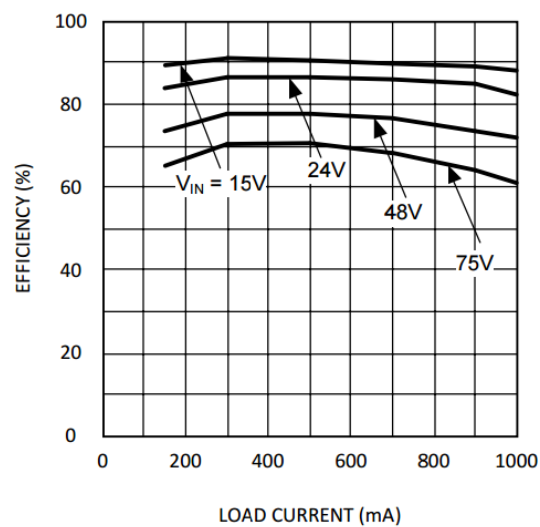


Figure 2.11: Efficiency vs. Load Current and V_{in} curves for LM5010 regulator (adapted from [66])

2.6.3 Logic Architecture

The design changes to the logic for the integrated version are presented below.

2.6.3.1 MCU, Bluetooth and IMU

The microcontroller, Bluetooth and IMU modules were integrated onto the PCB as part of the requirement to design all electronics onto one board. To prevent any loss of functionality provided by the COTS modules, the schematic of each was analyzed and the matching functionality was included on the integrated design.

The equivalent microcontroller to the Tiva C-series Launchpad is the TM4C123GH6PM, detailed below in Table 2.9.

Specification	Value
Vendor	Texas Instruments
Model	TM4C123GH6PM
Family	Tiva TM4C123x
Architecture	ARM Cortex-M4
Max Operating Frequency	80 MHz
Dhrystone MIPS Performance	100
Operating Voltage	3.3V
Max Current Consumption	58.7mA
Package	TQFP-64
GPIO	43

Table 2.9: Microcontroller Specification [50]

The microcontroller takes advantage of all GPIO from its direct placement on the board. Two user buttons, two user LEDs and a reset button were added to maintain compatibility with the Launchpad. The primary purpose of these buttons was to provide means of interacting with the hardware without the control tablet, such as during unit testing. Two crystal oscillators, one operating at 16MHz and another at 32.768MHz, provide the same clocks to the integrated design as the Launchpad, obviating the need for any code changes.

The corresponding module on the RN42-XV Bluetooth module was the Roving Networks RN42, and the Sparkfun IMU fusion board used an Analog Devices ADXL345 and InvenSense ITG3200. To troubleshoot the Bluetooth functionality, two LEDs are provided to indicate the connection status and state (e.g. discoverable, command mode) of the module. As the module is permanently bonded to the board, to recover from misconfiguration, a jumper is provided to restore the factory default settings of the module.

For each of the three modules, bypass capacitors were added as per vendor specification in order to maintain power integrity and a low-impedance power source path [67].

2.6.3.2 Level Shifting Subsystem

The Tiva operated on 3.3V logic; however, for several system peripherals, such as the servomotor drives, 5V logic was used. To interface between the two voltages, two level shifting ICs were chosen. For shifting from 5V down to 3V3, the TI SN74LVC4245A [68] octal bus transceiver was implemented; and for 3V3 up to 5V, the TI SN74LV4T125PWR [69] quadruple bus transceiver was implemented. Different chips were utilized due to requiring 6 outputs and 4 inputs, respectively; however, it is possible to also use the SN74LVC4245A for both. The SN74LV4T125PWR was attractive for its smaller TSSOP-14 package. Using the same chip for both purposes reduces the items on the Bill of Materials (BOM) and benefits larger production runs.

2.6.3.3 Expansion Port and Board Level Control Interface

To allow for system extension and reconfiguration, several interfaces were included on the board as provisions for new peripherals. This is chiefly accomplished through a dedicated expansion port. Listed in Table 2.10, the expansion capabilities of the board include an 8-bit wide unbuffered port,

a dedicated I²C bus and a 3.3V UART console header for local interfacing. These pins may be programmed in firmware to take on any alternate functionality provided by the microcontroller, with the exception of the I²C bus due to the pull-up resistors; these may be used with open-drain logic or de-soldered for general purpose IO.

Connector – Pin	Function	MCU Pin	Alternate Function				
			UART	SPI/I2C	CAN	ANALOG	MISC
CN14-11	EXPNO	PA0	UART0RX		CAN1RX		
CN14-13	EXPN1	PA1	UART0TX		CAN1TX		
CN14-15	EXPN2	PD4	UART6RX				USB0DM
CN14-17	EXPN3	PD5	UART6TX				USB0DP
CN14-19	EXPN4	PE1	UART7TX			AIN3	
CN14-21	EXPN5	PF1		SSI1TX			T0CCP1
CN14-23	EXPN6	PF2		SSI1CLK			T1CCP0
CN14-25	EXPN7	PF3		SSI1FSS			T1CCP1
CN14-27	I2C1	PB3					
CN14-29	I2C1	PB2					
CN13-1	TTY	PE4	(U5RX)	I2C2SCL	CAN0RX	AIN9	M0PWM5
CN13-2	TTY	PE5	(U5TX)	I2C2SDA	CAN0TX	AIN8	M0PWM4

Table 2.10: Expansion Port and Console Header Signal Mappings

Hardware opportunities for this expansion port include:

- Connection to slave microcontrollers or FPGAs for additional processing capability. FPGAs have been used in robotics [10, 70, 71] to eliminate computational bottlenecks.
- Communication with additional motor axes via CAN bus or RS-485 via a UART to RS-485 transceiver.
- GPIO expansion, via slave microcontroller, FPGA, bus expander or direct connection.
 - This would allow, for example, EMG sensors for robotic control, such as in [7, 72].
 - This would also allow for the device to be controlled by local buttons. One general observation about the existing exoskeleton platforms is the lack of redundant controls. The Ekso GT, ReWalk, ARKE, and HAL offer one primary means of

control, whether wired or wirelessly. This option would allow for simultaneous wired and wireless control options.

- This could also be used to couple instrumented force-sensitive crutches, such as in [73], into the device control system.
- Additional MEMS sensors.
- USB host or slave.
 - This would provide a high-speed general-purpose wired connection to control devices, human interaction devices, or for non-volatile data storage e.g. USB keys.
- Volatile or non-volatile data storage, such as external flash memory.

2.6.3.4 JTAG

The Launchpad contained a USB JTAG emulator using a second Tiva TM4C123GH6PM microcontroller [56]. This was used to program and debug the main microcontroller. Since the code for the JTAG MCU was not made available by Texas Instruments, an on-board debugger could not be included in the Integrated design; however, an external header on the Launchpad (Figure 2.12) enabled it to program and debug other targets.

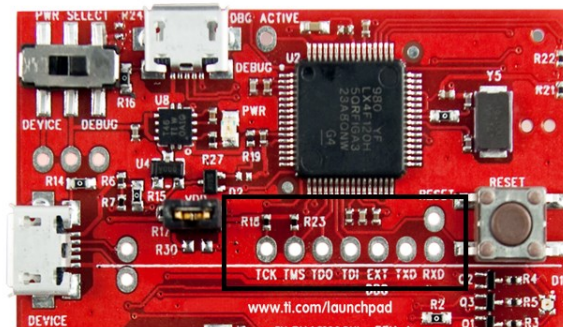


Figure 2.12: JTAG port on Tiva C-Series Launchpad (adapted from [52])

It was therefore decided to reuse the Launchpad as a JTAG emulator for the Integrated Design. The full connection is shown in Figure 2.13. Since the Launchpad has regulated 5V and 3.3V rails available, these may be used to optionally supply power to the target board and program it without the main HVDC supply present. Similarly, an external power supply may also be used providing that all voltages are earth referenced. However, in order to avoid power supply contention, power must not be supplied to any rail already energized by an onboard regulator. In addition, the VDD jumper must be opened on the Launchpad to disable power to the Tiva on the Launchpad which prevents a target conflict between the Tivas on the Launchpad and controller board. A connection to TX and RX lines are not required; however, programs which use UART0 for debugging messages will not be able to communicate to the host.

The JTAG connection is only necessary for programming and debugging. It may be disconnected during normal operation.

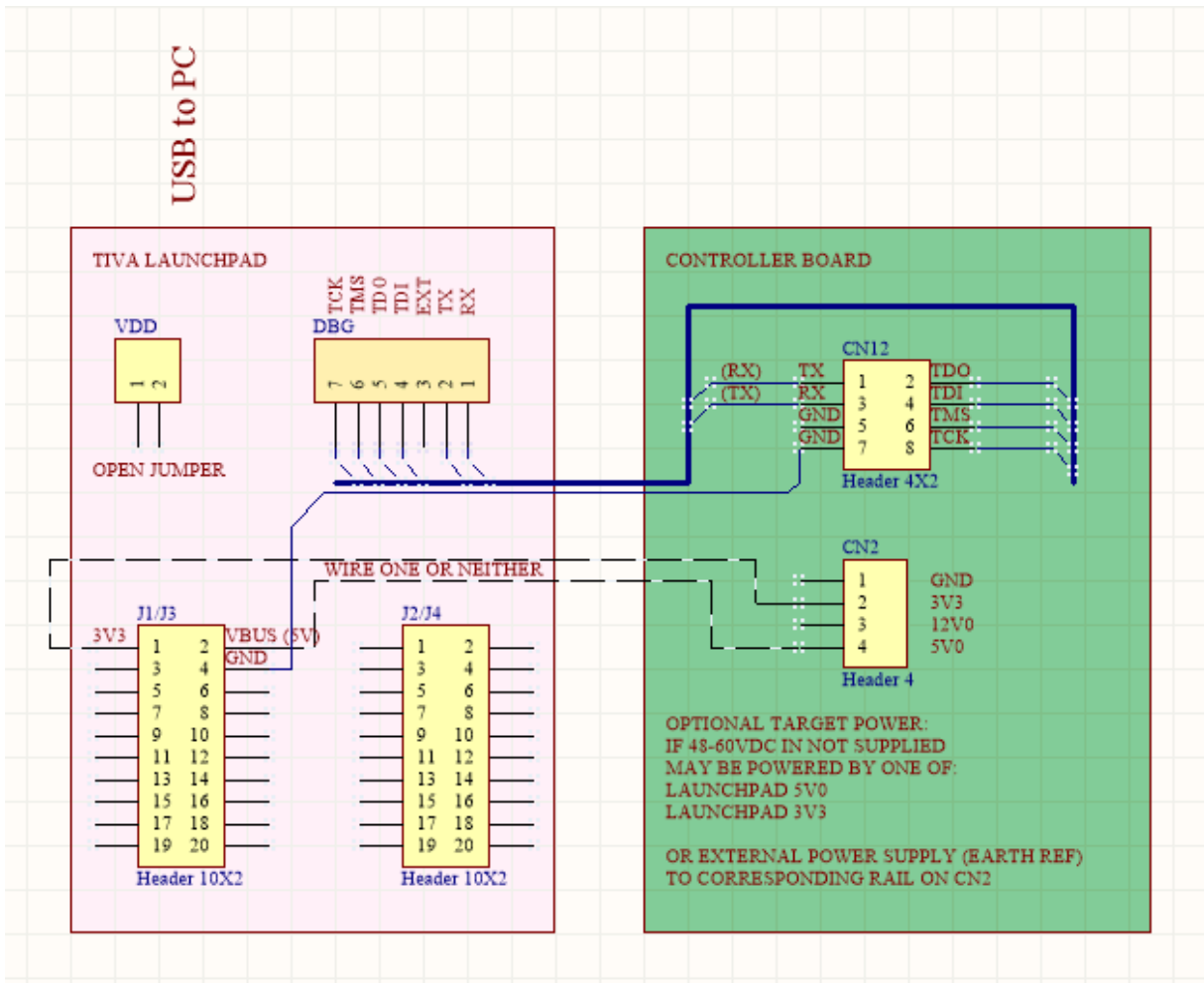


Figure 2.13: JTAG Connection to PCB

2.6.4 Block Diagrams

Figure 2.14 shows the block diagram of the Integrated design, summarizing the onboard functionality.

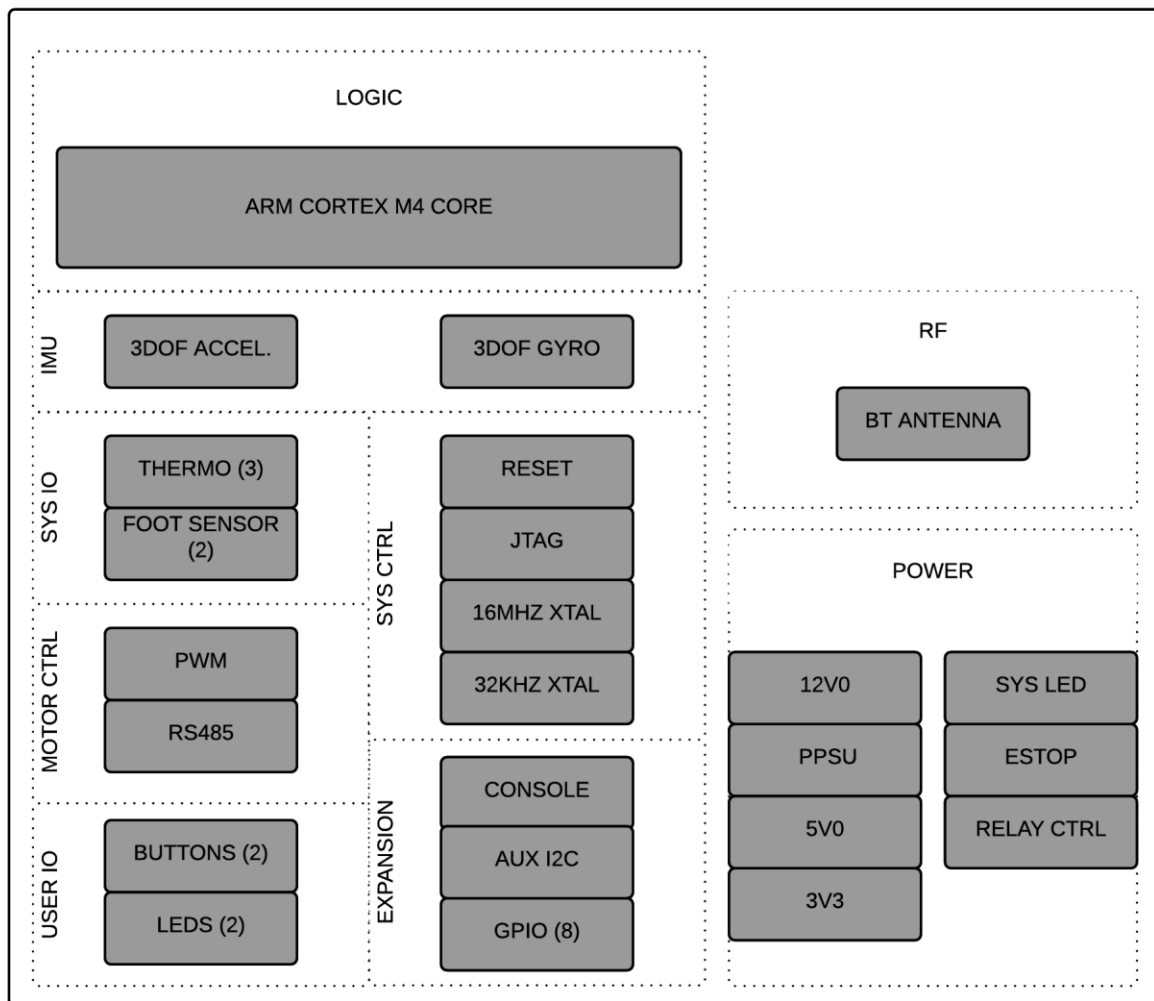


Figure 2.14: System Block Diagram of Integrated Design

The system block diagram is updated with the Integrated design, shown in Figure 2.15, for comparison with the Preliminary design shown in Figure 2.9.

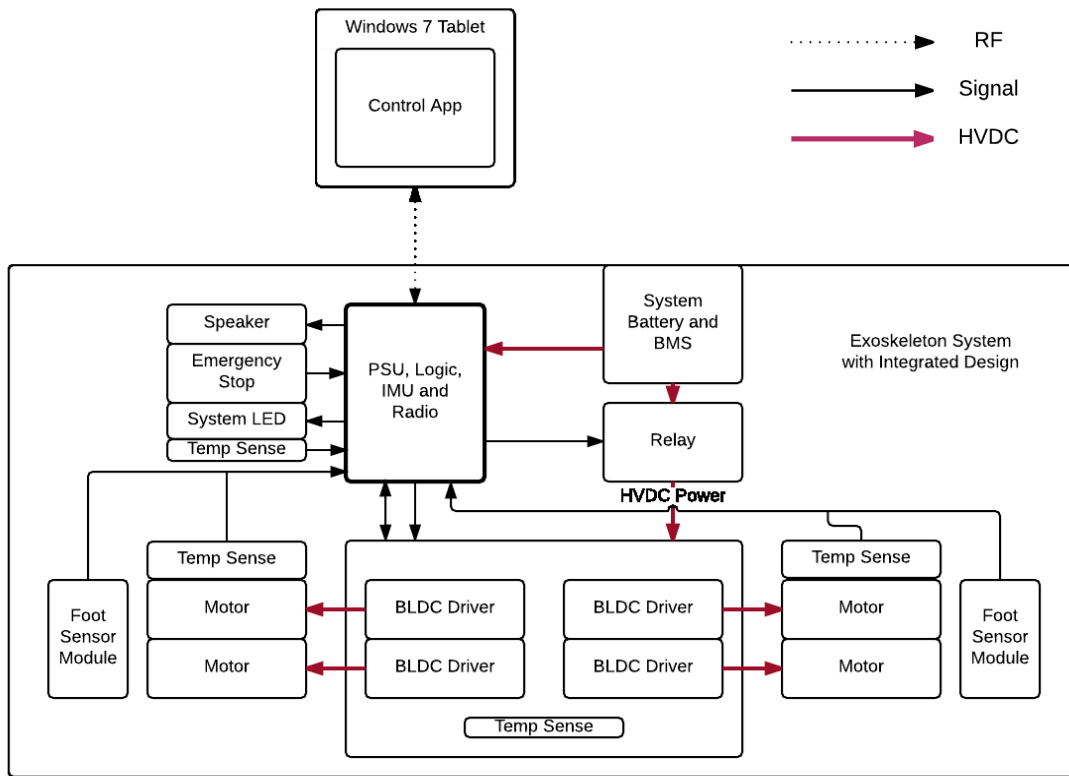


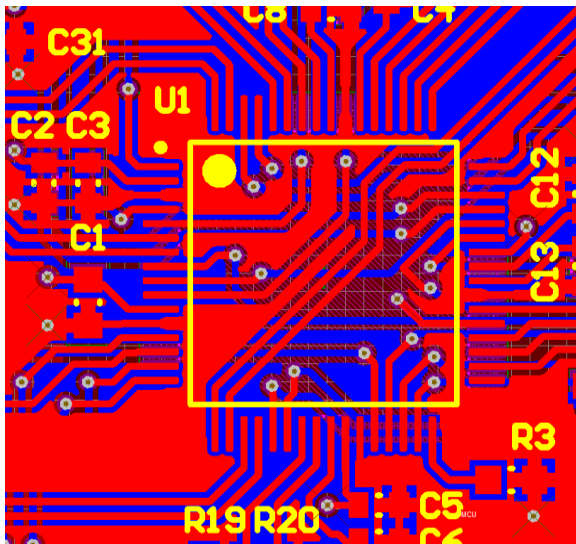
Figure 2.15: Block diagram of system with Integrated Design.

2.6.5 PCB Layout and Model

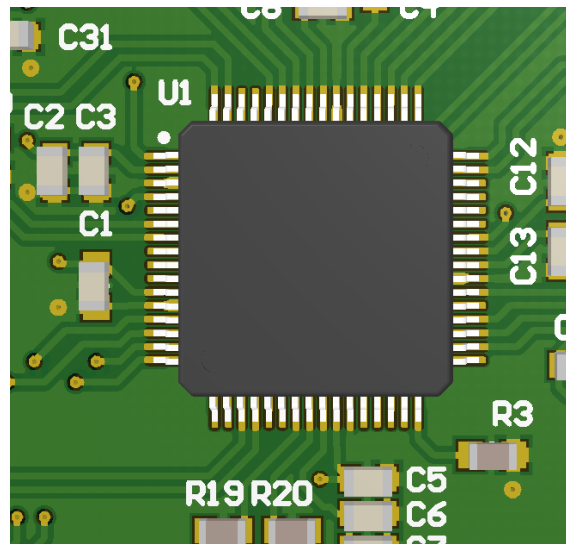
The PCB layout involved the placement of schematic components and routing of their interconnections. Figure 2.16a and b show a section of the PCB design in Altium as an example containing the microcontroller in 2D and 3D views, respectively.

One convenient feature of Altium is its content vaults with premade components for use in designs. However, the usefulness of these vaults is typically limited to passive components and large manufacturers due to the sheer variability of components available. As expected, this design required the creation of custom footprints and models. PCB modelling was undertaken to verify proper dimensioning and fit for components. For ICs, Altium provides an IPC compliant footprint tool for the generation of parts using common packages such as SOIC, TSSOP, TQFP, QFN, etc.

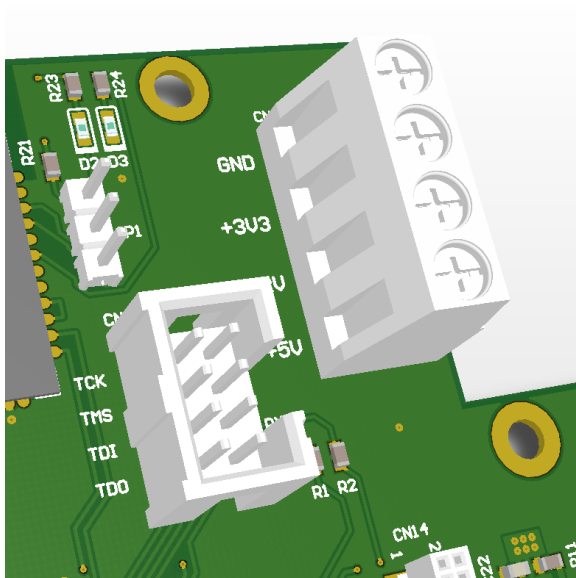
For connectors and other parts, the footprints were generated manually and coupled with a vendor-provided 3D model of the part such as in Figure 2.16c. For non-IC parts which did not have vendor-provided CAD models available, the parts were modeled using basic extrusions such as the capacitor in Figure 2.16d.



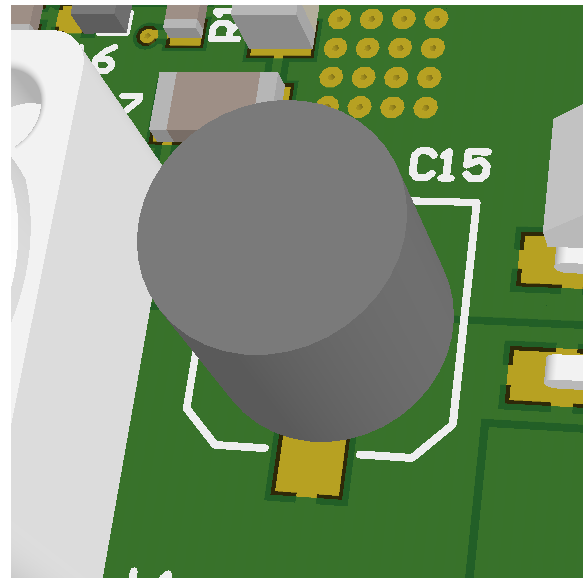
(a)



(b)



(c)



(d)

Figure 2.16: (a) top left: 2D layout of Microcontroller; (b) example of 3D model of part provided in Altium Vault; (c) examples of 3d models of parts provided by part vendor, (d) example of simple self-modeled part

Figure 2.17 shows an isometric render of the finalized layout of the Integrated PCB. The PCB was designed using a standard 4-layer stackup using 1-oz copper on FR4. This is detailed in Appendix A. Four layers were chosen to provide large, low-impedance copper pours for the power and ground planes, and had the most attractive tradeoff between ease of layout and cost. FR4 was chosen due to its suitable thermal performance; while high Tg (glass transition temperature) FR4 materials exist (e.g. isola370), they were deemed unnecessary for the heat dissipation expected of the components.

To minimize ohmic losses, the voltage regulators are clustered together, minimizing the distances between output-to-input, and, to provision for a heatsink, the LDOs are placed next to two mounting points. This is in contrast to the Preliminary design where regulators were on separate boards.

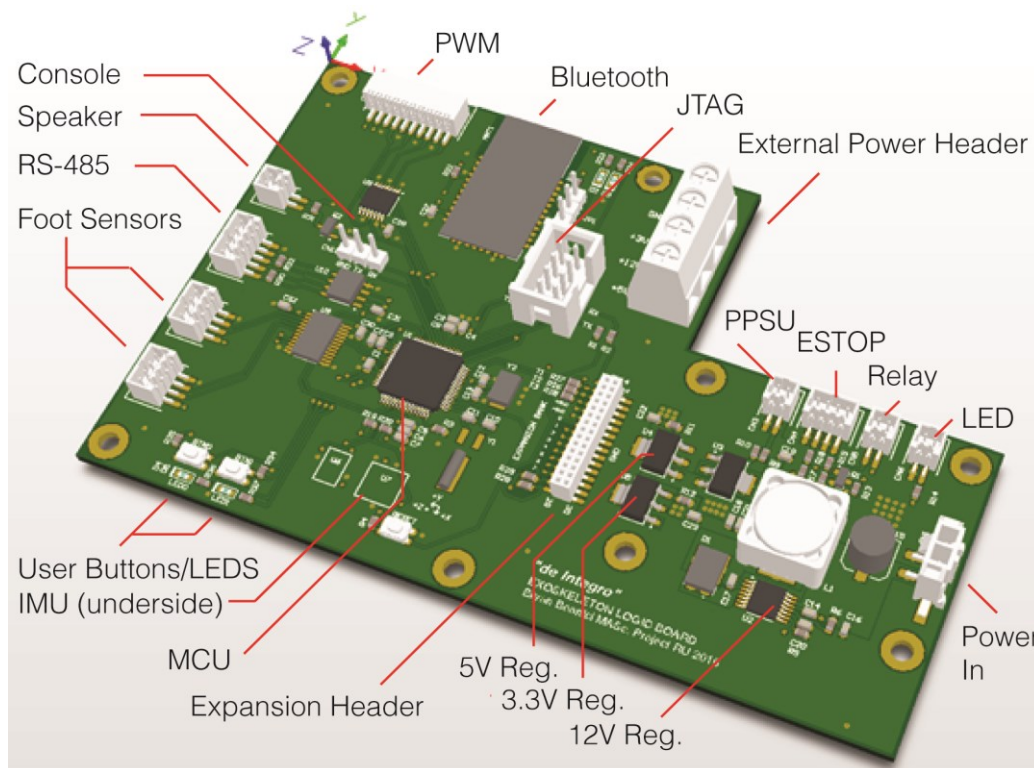


Figure 2.17: 3D Isometric view of Integrated Design showing components and system interfaces

The dimensions of the bare and populated PCBs are listed in Table 2.11. For populated PCB, the volume was measured as the smallest bounding box that would enclose the PCB. This is listed with the surface area in Table 2.12.

	Dimension	Value	Unit
Bare PCB	X	1250 (490 cutout)	mm
	Y	800 (300 cutout)	
	Z	1.59	
Populated PCB	X	12.50	
	Y	8.00	
	Z	13.50	

Table 2.11: Dimensions of Integrated Design

Parameter	Value	Unit
Surface Area	8530	mm ²
Volume	115200	mm ³

Table 2.12: Surface Area and Volume of Integrated Design

2.7 SUMMARY

The operation of an exoskeleton was discussed and the Preliminary architecture for its operation was presented. The drawbacks to the design were discussed from power and signal integrity, extensibility and reliability perspectives, motivating the design for an integrated platform. The design of the integrated platform which remedies these deficiencies was introduced and modelled. In Chapter 3, this design is constructed and verified for operation.

3 FABRICATION AND TEST OF INTEGRATED DESIGN

3.1 INTRODUCTION

This chapter presents the steps taken to assemble and test a unit of the Integrated design and the verification process used at all stages of fabrication. This is done to prepare the boards for system installation and data collection discussed in Chapter 4. The results of unit tests will also be discussed.

3.2 VALIDATION METHOD

Three bare boards of the Integrated design were fabricated and one assembled for in-system testing. In order to ensure the proper functionality of the boards prior to placement in the system, the following testing sequence was devised:

- 1) Design Verification – Verifying that the PCB meets the specification before it is manufactured
- 2) Vendor Selection – Choosing the supplier for the PCB
- 3) Bare Board Inspection and Test – Verifying that the bare PCBs were manufactured correctly
- 4) Assembly – Placing and reflowing the components onto the PCB
- 5) Post Reflow Inspection and Test – Verifying that the reflow was performed correctly, correcting faults
- 6) Unit Testing and Integration – Verifying that subsystems work as designed and interconnecting them

- 7) Flashing – Programming the PCB with the production firmware
- 8) System Integration – Placing the PCB in the system for testing

Ensuring that the board is operational is essential for the validity of the experimental data.

3.3 DESIGN VERIFICATION

Prior to manufacturing, the integrated PCB layout was checked for errors which could cause the design to fail, such as insufficient net and component clearances, overlaps and unrouted connections in a process known as the Design Rules Check (DRC). The DRC report and settings are tabled in Appendix A. Unlike Eagle, Altium provided online DRC which highlighted errors as they were made and routed traces according to the set DRC rules. This minimized the number of iterations required before the design had zero DRC errors.

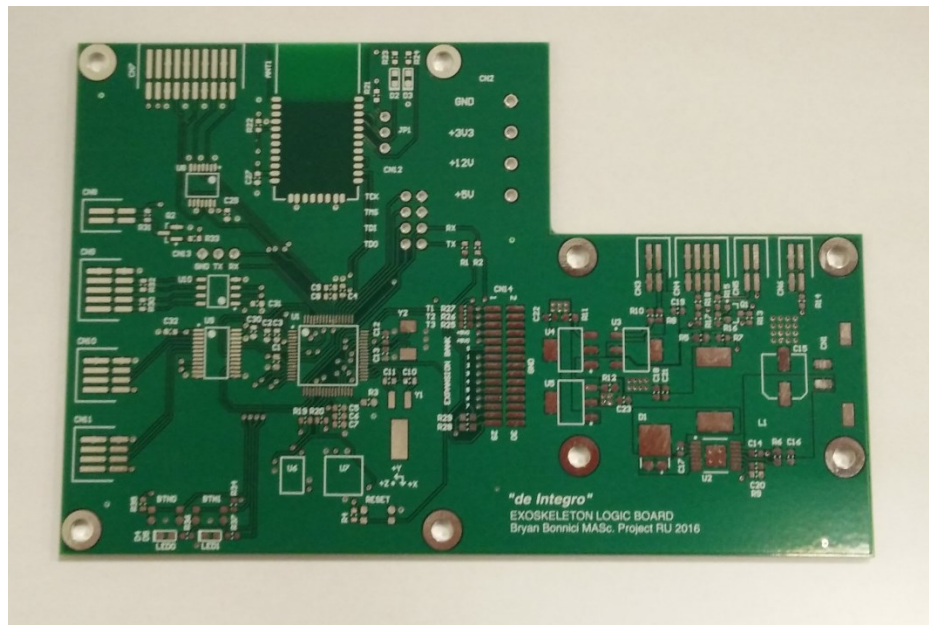
The DRC rules were configured to match the requirements for the student discount program of Advanced Circuits, the PCB vendor, in order to minimize rejection by the vendor's CAM department. Specifically, the minimum trace-space clearance was restricted to 10mil each and via sizing was restricted to 15mil minimum diameter with 5mil annular ring.

3.4 VENDOR SELECTION

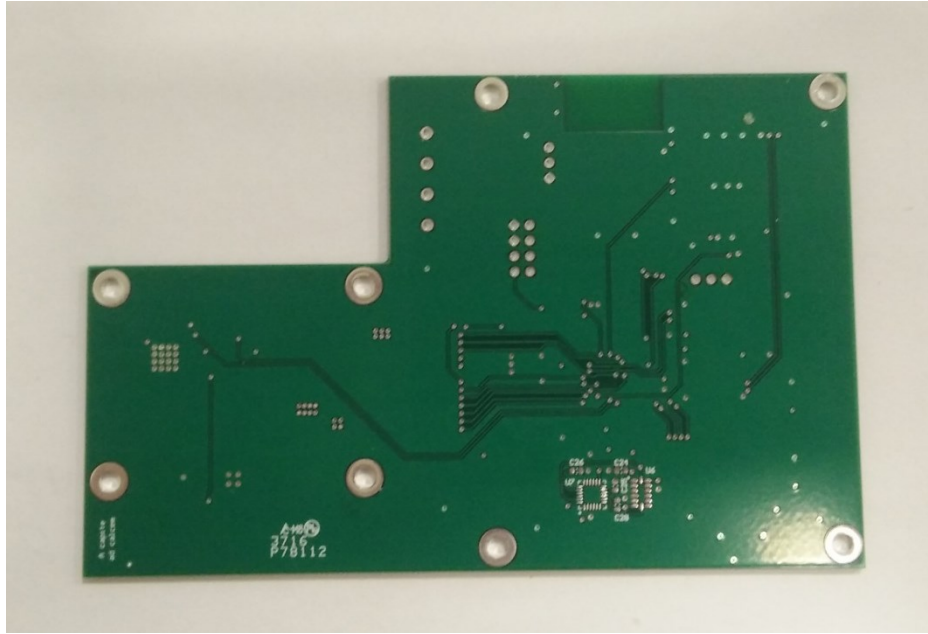
Advanced Circuits were chosen as the PCB vendor as they were the lowest-cost ISO 9001-2008 fab which could manufacture low volume PCBs to IPC-A-600 Class 2 specification with turnaround times of less than two weeks.

3.5 BARE BOARD INSPECTION AND TEST

While the PCB vendor performed a 100% netlist electrical test for isolation and continuity on each board prior to shipment, an independent check of continuity and isolation for select power and signal nets was performed as an additional layer of diligence prior to assembly in order to eliminate manufacturer error should issues arise at later stages of fabrication. The continuity test was performed at an anti-static workstation with a Fluke 87-V multimeter. The bare boards are shown in Figure Figure 3.1 and the results of the tests are listed in Table 3.1.



(a)



(b)

Figure 3.1 a) Top side and b) Bottom side of the bare board.

Test	Result
Continuity Test on Power and Signal Nets	PASS
Isolation Test on Ground and Signal Nets	PASS

Table 3.1: Results of electrical test on unpopulated PCBs

3.6 PCB ASSEMBLY

Following bare board inspection, the boards were assembled. The following steps detail the method used for populating and reflowing each PCB. Assembly was performed at an anti-static workstation with a microscope, IR Reflow Oven (detailed in Appendix B), and PCB reworking tools. Custom stencils (supplied by OSH Stencil), generated alongside the board production files from Altium, were used to apply the solder paste to the pads.

1. The bare PCB was placed bottom-side up on the working surface and the stencil jig was secured tightly to the board edges. The jig was secured to the working surface using Kapton tape. The bottom-side was chosen first since it has a few small components. This approach minimized the risk of the small components falling off when the top-side was reflowed.
2. The bottom stencil was aligned with the PCB under a microscope and fastened to the jig with Kapton tape.
3. Room-temperature 63Pb-37Sn solder paste was spread onto the stencil with a disposable applicator ensuring even deposition on all pads. Note: Leaded solder was chosen for its lower reflow temperature in order to maximize the temperature safety margins to components during reflow. For RoHS compliance, an unleaded alloy paste such as SnAgCu could be substituted. The bare PCBs use an unleaded HASL finish.
4. The stencil was lifted to check the alignment of paste. If the paste was misaligned, the board was cleaned with isopropanol 97%, placed under a realigned stencil and the paste reapplied.

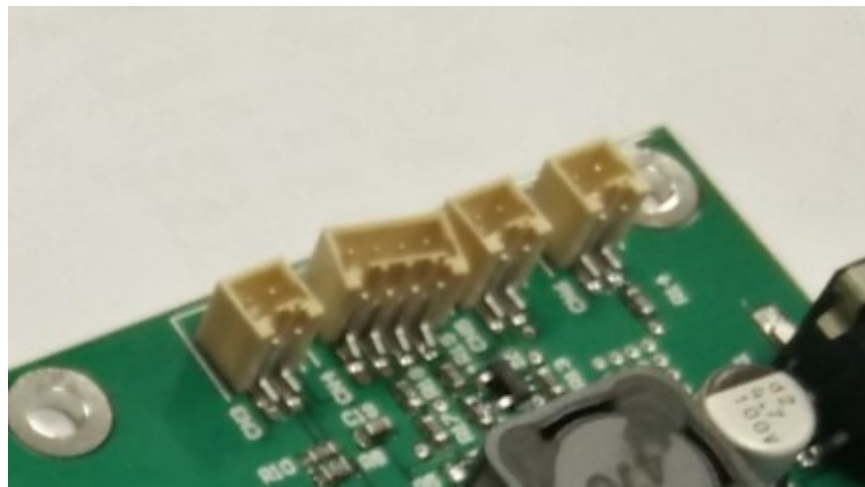
5. Using tweezers and a microscope, the bottom-side SMD components were placed individually.
6. The PCB was moved to an IR oven and reflowed using an unleaded solder profile. Appendix B describes the oven and the specific settings used.
7. The PCB was removed from the oven and inspected for defects. The defects were reworked as necessary.
8. The board was flipped over and steps 1-7 were repeated for top-side SMD components using the top-side stencil. Approximately 2mm height was added to the jig to compensate for the offset height of the bottom-side components. The jumpers connecting the output of each regulator were not populated at this time. These were left unconnected for testing and were applied once it was verified that the regulators were working properly.
9. All through-hole components were manually soldered using tack flux, 63Pb-37Sn solder wire, and a soldering iron set to 500°F.

3.7 PCB POST-ASSEMBLY INSPECTION

The PCB was visually inspected under a microscope for defects that may have developed during reflow such as solder bridges and ‘tombstoning.’ Several defects were found bridging the legs of various ICs together (Figure 3.2a) and one connector was pulled askew during the reflow (Figure 3.2b). These faults were corrected manually with a soldering iron. The PCB was free of tombstoning faults or un-reflowed components.



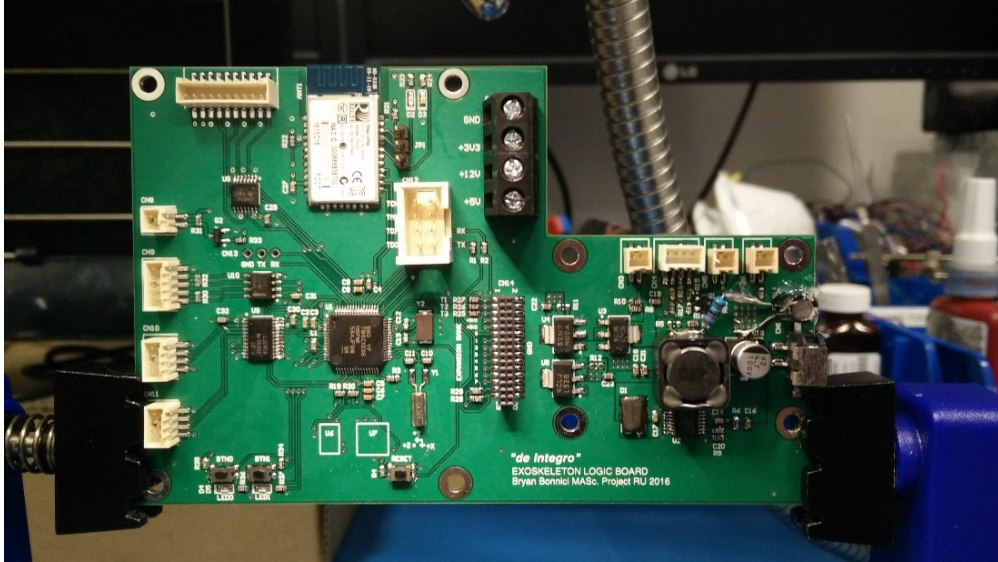
(a)



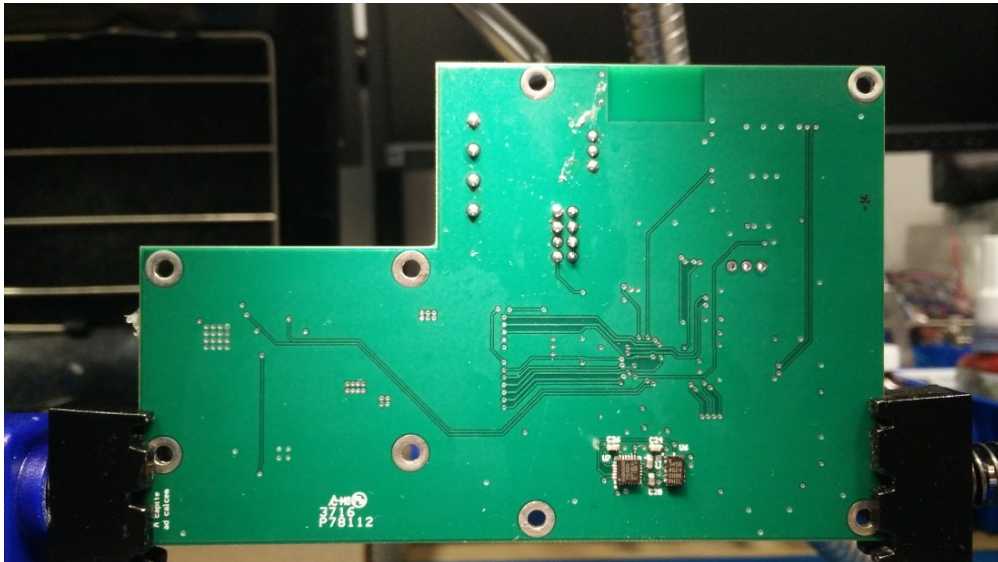
(b)

Figure 3.2 a) Various solder bridges are present across IC legs after reflow, b) A connector pulled askew during reflow.

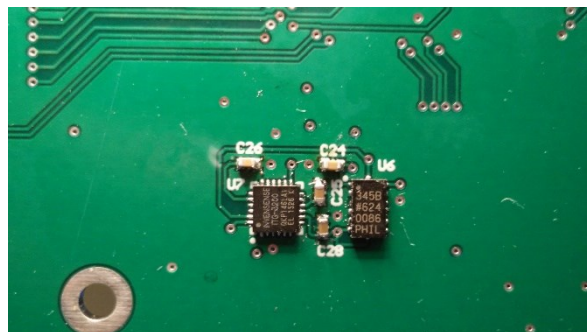
Figure 3.3 shows the fully assembled boards. The boards closely resemble the models presented in Figure 2.17.



(a)



(b)



(c)

Figure 3.3 a) Assembled top side of PCB, b) Assembled bottom side of PCB, c) Close-up of IMU

3.8 PCB POST-ASSEMBLY ELECTRICAL TEST

After visual inspection, the PCB was tested again for isolation and continuity on all power nets and key signal nets with a Fluke 87-V DMM. This stage was done to detect any possible faults that may have been missed during visual inspection. This stage was critical to prevent damage to components when power applied. The test results are shown in Table 3.2.

Test	Result
Continuity Test on Power and Signal Nets	PASS
Isolation Test on Ground and Signal Nets	PASS

Table 3.2: Results of Post-assembly PCB testing

3.9 UNIT TEST AND INTEGRATION

3.9.1 Initial Power On

At this stage, the assembled PCB was ready for initial power-on. The PCB was connected to the Launchpad as per Figure 2.13 with an external 150mA current-limited earth-referenced power supply providing 3.3V. The Launchpad was connected to a PC installed with two Texas Instruments Software SDKs:

1. Energia, an Arduino-like IDE for quick peripheral unit tests, and
2. Code Composer Studio V6 with TivaWare for advanced debugging and programming.

A “blink” program was written in Energia to alternately flash the two User LEDs on the Device Under Test (DUT) every second. Figure 5.2 shows the DUT connected to the Launchpad and external 3V3 power supply running the program.

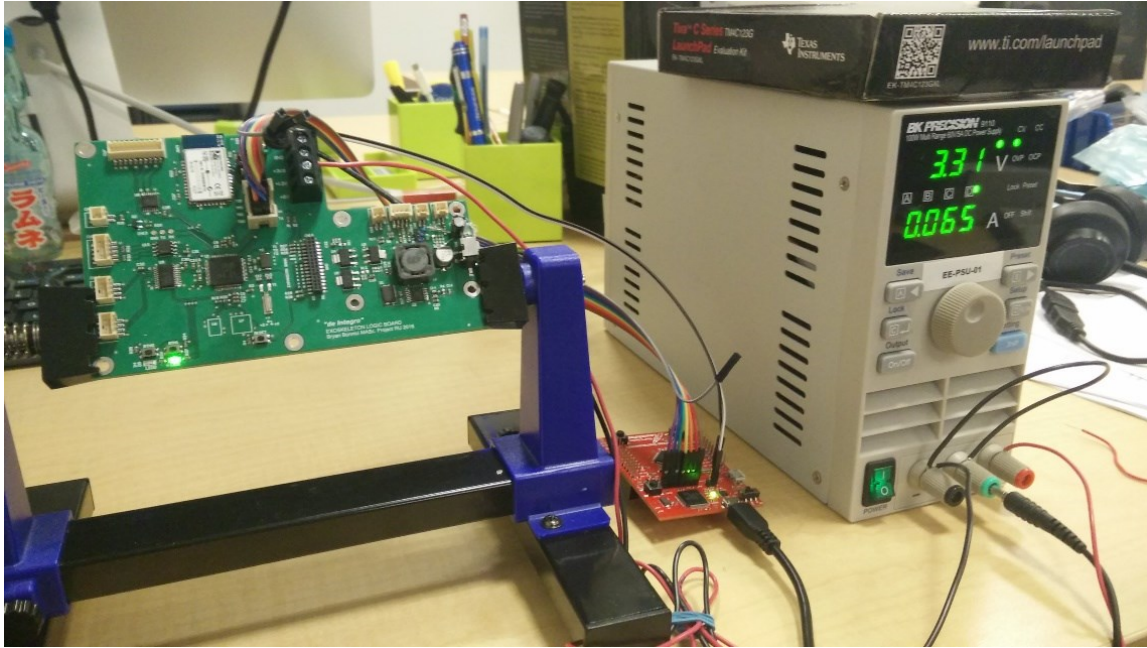


Figure 3.4: Initial programming of the microcontroller. The microcontroller is loaded with the blink program. The LED on the lower left of the board is illuminated and flashes with the adjacent LED.

The main oscillator of the microcontroller was probed using a Tektronix MSO2024B oscilloscope to verify that the microcontroller was being driven from a correct frequency of $f_{osc} = 16\text{MHz}$.

3.9.2 Power Supply Verification

Each regulator of the DUT was independently tested before their outputs were connected to their respective power planes on the PCB. This was done to prevent damage to downstream components in the event a regulator did not function as designed. In such case, the defective output could be supplied by an external supply through the external power header. Power was applied using a B&K Precision 9110 DC power supply through the external power header to the inputs of the regulators. For the 12V, 5V and 3.3V regulators, these voltages were 60.00V, 12.00V and 5.00V, respectively. The output voltage was measured without load using a Fluke 87-V DMM.

It was discovered during the test that a capacitor was needed for the output of the 12V0 buck converter to function properly. A 1 ohm radial resistor and 22uF capacitor were added in series to ground as shown in Figure 3.5.

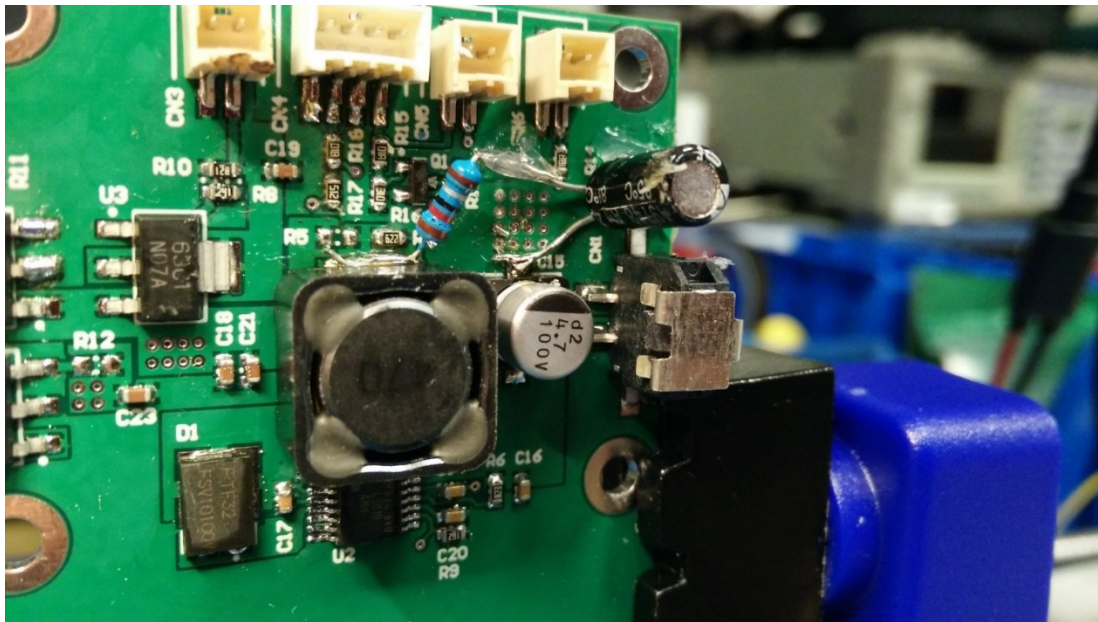


Figure 3.5: Reworked Buck Converter

The buck converter was measured on the oscilloscope to verify that the ripple voltage ΔV_{out} did not exceed 600mV (Nominal ± 300 mV), shown in Figure 3.6.

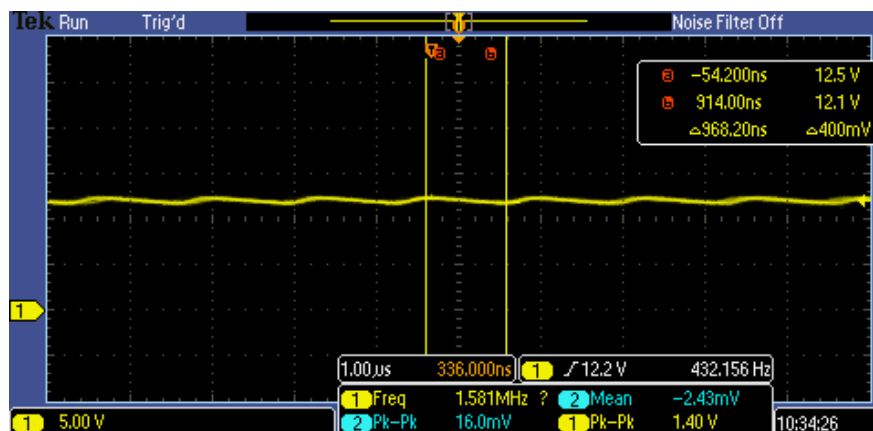


Figure 3.6: Output of 12V0 buck converter

All power supply tests and their results are summarized in Table 3.3.

Test	Result
12V0 rail is $12.0V \pm 300mV$ (unloaded)	PASS
12V0 rail is $12.0V \pm 300mV$ (500mA load)	PASS
PPSU/5V5 rail is $5.5V \pm 100mV$ (unloaded)	PASS
PPSU/5V5 rail is $5.5V \pm 100mV$ (150mA load)	PASS
5V0 rail is $5.0V \pm 150mV$ (unloaded)	PASS
5V0 rail is $5.0V \pm 150mV$ (100mA load)	PASS
3V3 rail is $3.3V \pm 100mV$ (unloaded)	PASS
3V3 rail is $3.3V \pm 100mV$ (150mA load)	PASS

Table 3.3: Summary of Power Supply Tests

Voltage was applied using the external power header. Once each power supply was tested and validated, the DUT was powered down and jumpers were soldered to connect the regulator outputs to the logic of the DUT.

3.10 ADDITIONAL PERIPHERALS

3.10.1 Foot Sensors

The foot sensors for the device were unit tested with firmware that illuminated a user LED when the corresponding sensor was occluded. This is shown in Figure 3.7.

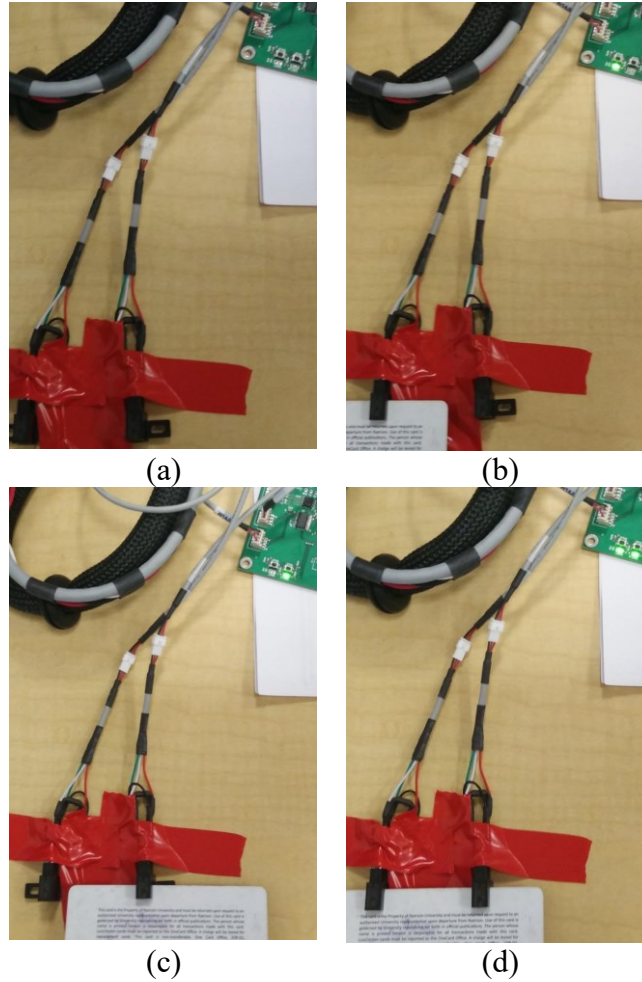


Figure 3.7 Testing the foot sensors. The left and right LEDs on the board illuminate when their respective foot sensor is occluded. a) Both sensors open, b) Left sensor occluded, c) Right sensor occluded, d) Both sensors occluded.

The test results are summarized in Table 3.4.

Test	Result
LED0 asserts only when left sensor is occluded	PASS
LED1 asserts only when right sensor is occluded	PASS

Table 3.4: Summary of Foot Sensor Unit Test

3.10.2 System Control

It was also necessary to test the Emergency Stop and System Power LED functionalities before placement in-system. To test the Power LED, the LED was connected and the nominal input voltage was applied to the board. The voltage at the anode of the LED was observed on an

oscilloscope. The status of the LED was required to match the presence of input power to the board. To test the Emergency Stop, the button and relay were both connected to their respective points on the board and the resistance of the relay was measured for both states of the button. The results are listed in Table 3.5.

Test	Result
Pressing the Emergency Stop deactivates motor power	PASS
Releasing the Emergency stop reactivates motor power	PASS
System power LED is on at all times when power is engaged	PASS
System power LED turns off within 500 ms when power is disengaged	PASS

Table 3.5: Summary of System Control Unit Tests

3.10.3 Bluetooth Configuration

In the Preliminary design, the Bluetooth module was connected by a standard 10x2mm socket typically used by 802.15.4 radio modules and could therefore be programmed using any standard USB to 10x2 pin adapter or USB to TTL serial cable. In the integrated design, the Bluetooth system is assembled directly onto the PCB, necessitating that programming be done through the main microcontroller. A code was developed to emulate a serial terminal on the main microcontroller which configured the Bluetooth module over 115200 baudrate, 8N1 connection to use “ExoBoard” as SSID, set serial port profile, and use a PIN. Figure 3.8 shows the BT module configured and advertising on an Android smartphone.

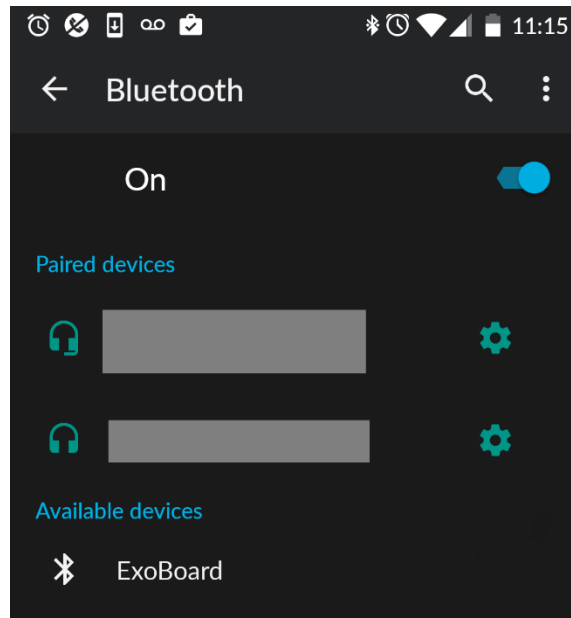


Figure 3.8: Integrated Design advertising over Bluetooth

3.11 FLASHING

With the board's subsystems verified, the system firmware could be loaded onto the microcontroller. The unit was programmed over JTAG with the ARKE firmware from Code Composer Studio.

3.12 SYSTEM INTEGRATION

The board was now ready to be placed in the system. The Integration of the board into the system is further discussed in Chapter 4.

3.13 CONCLUSION

A unit of the Integrated design was produced and passed all unit tests. The produced unit was readied for experimentation and data collection.

4 EXPERIMENT

4.1 INTRODUCTION

This chapter presents the experimental and data collection methods for testing the Integrated design. The board is placed in-system and walking trials are performed to gather data. Data is saved from the system API and imported into MATLAB for post processing. The results are discussed in Chapter 5.

4.2 EXPERIMENTAL SETUP

The experimental setup involves the placement of the design in-system and configuring the control tablet for use. This is required to be done on a per-system or per-tablet basis.

1. The integrated design was placed in-system and all internal connections were wired.
2. The exoskeleton was powered on.
3. The tablet was powered on.
4. The tablet was paired with the new board using the Windows 8 Bluetooth pairing interface.

Once the tablet was paired, the system was configured and ready for trials.

4.3 TRIAL PROCEDURE

The trial procedure describes the process for obtaining performance data from the system. The process follows the steps outlined in Figure 2.3.

1. The control application was started on the tablet and connected to the device.
2. A homing command was issued to the device.
3. Following homing, a “stand” command was issued to the device.

4. Operator control mode was initiated, and a walking sequence was initiated on the device.
5. After 40 steps, the walking sequence was terminated.
6. A “sit” command was issued.
7. Upon completion, the session was finished on the control tablet.
8. The device was powered off and the session data was saved and downloaded for analysis.

4.4 DATA COLLECTION AND POST PROCESSING

The following is a partial list of data sampled during walking sessions and logged to file by PatientProfile:

- Sample time stamp (ms since power on) (Integer)
- Position of each axis (deg) (Float)
- Velocity of each axis (deg/s) (Float)
- Torque of each axis (Nm) (Float)
- Forward and side tilt angles (deg) (Float)
- Device status and flags (Bit Field/Integer)

Data was sampled at approximately 50Hz. In addition, the travel distance, and number of steps taken and session time were recorded. This data was saved locally on the tablet as a CSV file. This file was transferred to a local workstation for analysis in MATLAB. A script was developed to read and plot the time, position and velocity vectors in the API data. These files were inspected and filtered to determine regions of interest.

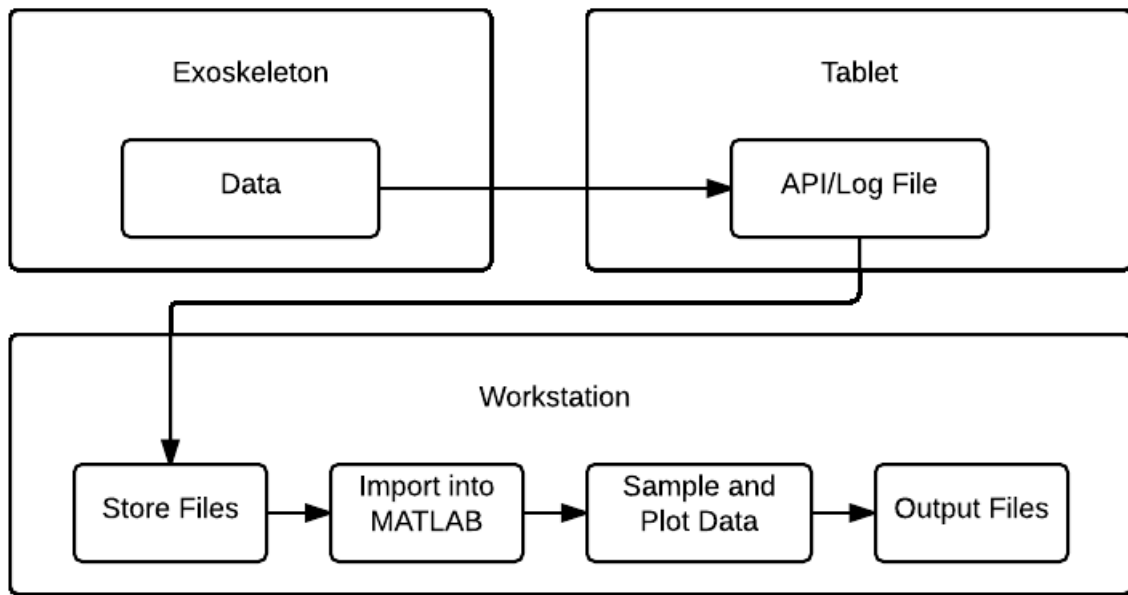


Figure 4.1: Workflow for collecting and processing walking session data

4.5 SUMMARY

This chapter provided the methodology for data collection and analysis of the performance of the Integrated design. Data was collected during walking trials and were used to compare with the one collected with the benchmark design. This is presented in Chapter 5.

5 EXPERIMENTAL RESULTS AND DISCUSSION

5.1 INTRODUCTION

This chapter is dedicated to the analysis and comparison of the Preliminary and Integrated designs. This chapter compares the performance and size of the two designs.

5.2 PERFORMANCE DATA

Figure 5.1 shows the random sampling of the device in operation with the Preliminary design. The waveforms for the sagittal joint angles and velocities are shown for each hip and knee. It can be observed that the waveforms shown in Figure 5.1 approximate the pathology-free gait as described in Figure 1.6. The time axis indicates the time in seconds since device is powered on. Since the device does not walk continuously, the area of interest is chosen to demonstrate four consecutive gait cycles.

The analyses are then repeated for the Integrated design, and the results are shown in Figure 5.2. As it can be seen in the figure, the device recreates a similar gait cycle.

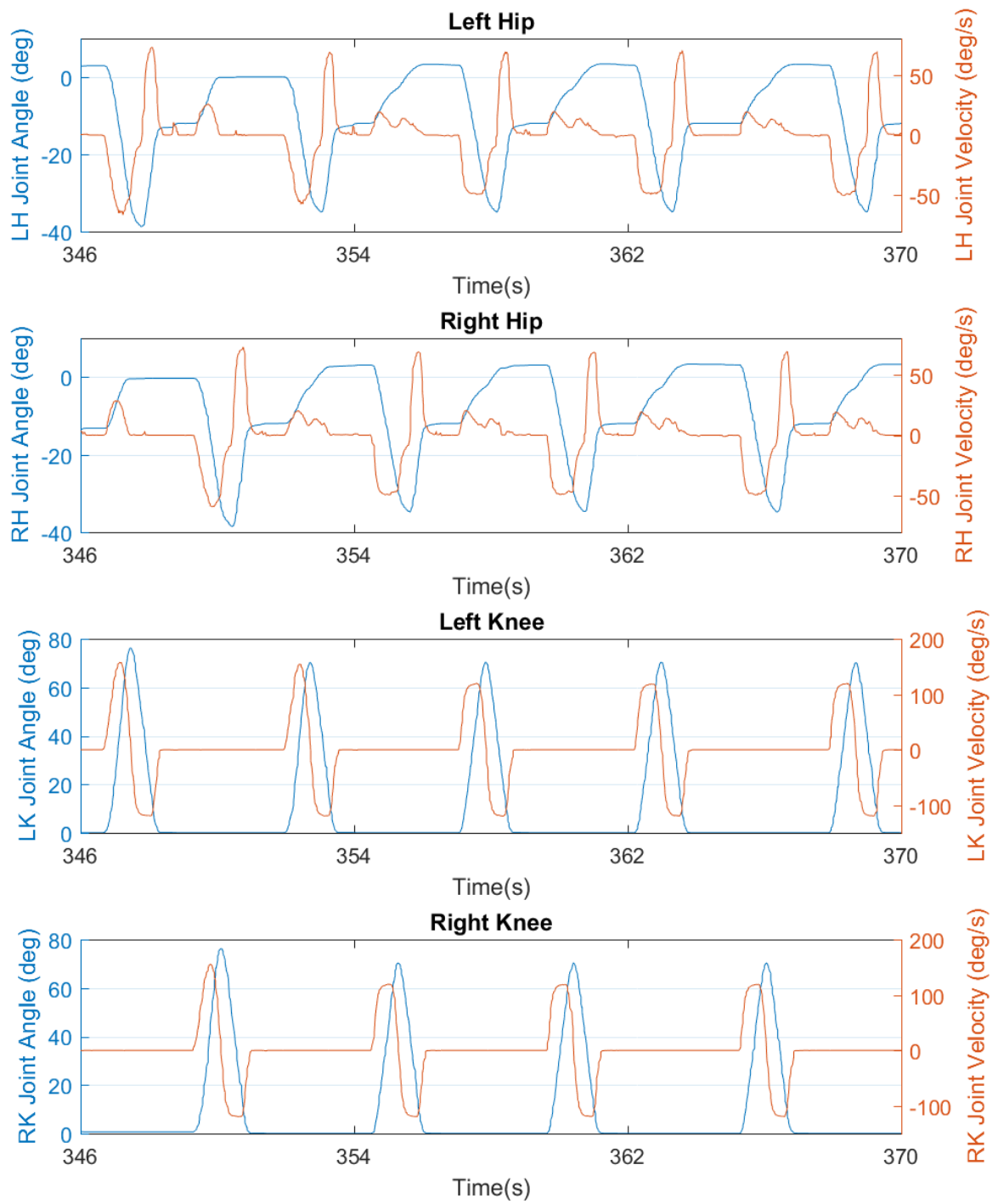


Figure 5.1: Joint angles and velocities of ARKE system using Preliminary Logic Board

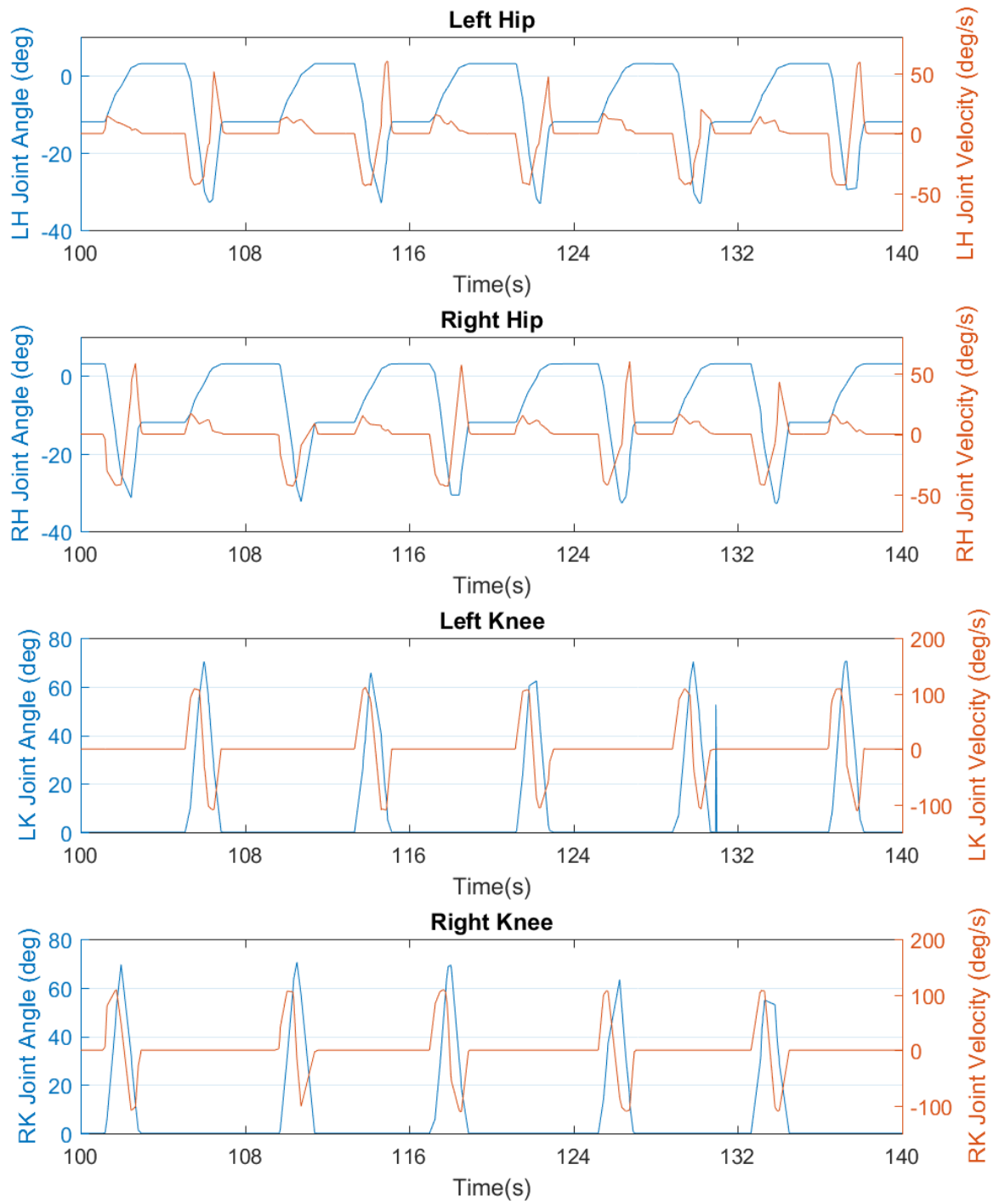


Figure 5.2: Joint angles and velocities of ARKE system using Integrated Logic Board

5.3 SIZE ANALYSIS

To estimate the footprint reduction of the new design, the dimensions of the Preliminary boards were measured and recorded. The X and Y dimensions of each board were obtained from Eagle CAD. Since Eagle does not have any 3D modelling capability, the Z (height) dimension of each board was measured using a calibrated Mitutoyo 500-196-20 digital caliper and was recorded as the height between the tallest components on each side in order to be consistent with the measurements of the Integrated design reported in Table 5.1.

Board	Dimension	Value (mm)	Surface Area (mm ²)	Volume (mm ³)
Logic Board (Assembled)	X	82.55	5346.76	129819
	Y	64.77		
	Z	24.28		
Power Board	X	49.21	1953.14	32559
	Y	39.69		
	Z	16.67		

Table 5.1: Dimensions of Preliminary Design

For surface area calculation, the dimensions of the modules were measured and listed in Table 5.2. Note that for the Bluetooth module, the X and Y dimensions are listed as the extents. However, since the board was not rectangular, the surface area is reflected as the actual area of the part as calculated from the datasheet.

Board	Dimension	Value (mm)	Surface Area (mm ²)
Tiva	X	63.50	3225.80
	Y	50.80	
IMU	X	15.24	251.61
	Y	16.51	
Bluetooth Module	X	24.40	603.28
	Y	29.90	

Table 5.2: Dimensions of COTS modules

The total measurements for the Preliminary design are tallied up in Table 5.3.

Parameter	Preliminary Design	Integrated Design	Δ	$\Delta\%$
Footprint	11380.60 mm ²	8530 mm ²	- 2850.6 mm ²	- 25.0
Volume	162378 mm ³	115200 mm ³	- 47178 mm ³	- 29.0

Table 5.3: Size comparison of Preliminary vs Integrated designs

The Integrated design achieves savings of 25% on total PCB area and 28% on PCB volume.

5.4 SUMMARY

This chapter compared the performance of the Integrated and the Preliminary designs in terms of functionality, size and cost. It was demonstrated that the Integrated design recreates the walking gait pattern while achieving a smaller size.

6 CONCLUSIONS AND FUTURE WORKS

6.1 CONCLUSIONS

The primary contribution of this thesis is a novel, compact, extensible hardware platform for fully assistive lower body exoskeletons. The integration of components onto one single PCB allowed the design to be represented in a 30% smaller space than the modular COTS-based prototype. The elimination of friction-fit connections and stacked boards increased signal integrity and mechanical robustness. Similarly, the elimination of COTS components allowed for expansion of functionality.

The design and assembly of the hardware platform was documented and the design was verified using an existing clinical exoskeleton. It is shown through experimentation that the design is able to recreate a pathology-free gait in the sagittal plane and fulfill the basic requirements of a lower body exoskeleton, achieving the outlined objectives. Pending additional validation and burn-in, this design is suitable for future deployment to human trials. In the future, this design can be used to drive smaller, more lightweight robotics.

6.2 IMPROVEMENTS

While the design achieved its objectives, the reworked RC network added in Figure 3.5 was incorporated into the design following its release to manufacturing. This is shown as R38, C33 in Figure 6.1.

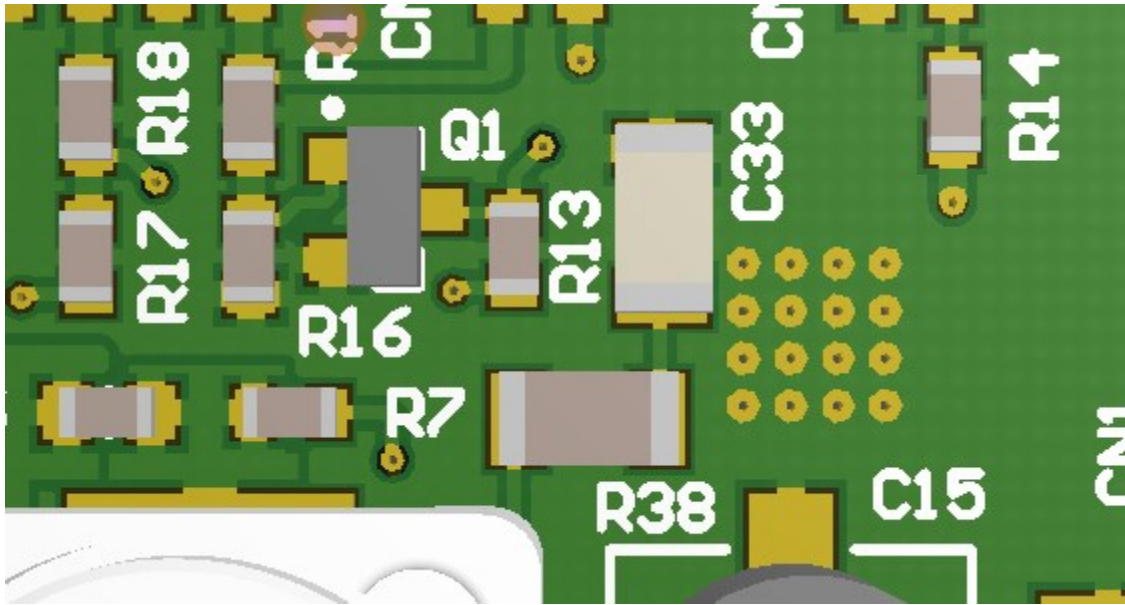


Figure 6.1: Addition of reworked RC network to PCB.

6.3 RECOMMENDATIONS AND FUTURE WORKS

The results of this study have produced a number of recommendations for future studies:

1. Thermal analysis using an imaging camera (e.g. FLIR) would provide insight into the heat performance of the board under normal operating conditions. This can be used to determine the effect of thermal fatigue on the design, and also to determine whether certain nets need additional width or layers need additional plating thickness.
2. Quantitative measurement on RF leakage and susceptibility of the boards would provide insight into the difference in EMI performance of the designs. Electronics must meet interference standards by Health Canada (US: FCC) before approval for sale. Of note, the specific absorption rate (SAR) limits of RF energy exposure must be below .08W/kg for

the whole body for frequencies ranging between 3kHz and 300GHz as defined by Health Canada in Safety Code 6 [74].

3. Similarly, the design should be analyzed for compliance with IEC60601:2013, the standard defining the basic safety and essential performance of medical electrical equipment. This is a requisite for licensure by the FDA or Health Canada for devices intended for home use [75].
4. Additional validation and testing is required to determine the safety and performance record, part of the risk assessment of the design, before human trials can begin. Further units should be assembled and burn-in tests should be performed.
5. Due to the varying delays between steps, software analysis could be advanced to overlay gait cycle on a normalized time basis, abstracting out the specific walking sequence used.
6. Via software, deep learning could be used on the API to track rehabilitation progress.
7. Using machine assembly, a more aggressive layout could be done with smaller passives such as 0402s, 0201s, and no-lead ICs/BGAs.
8. The Bluetooth PHY selected was not configured to encrypt communication, making it possible for an attacker to eavesdrop on communications or assert control via man-in-the-middle (MITM) attacks. Bluetooth Low Energy (BLE) provides Elliptic Curve Diffie-Hellman (ECDH) encryption as a core part of the specification which is effective at

thwarting these attacks [76]. Many off the shelf BLE modules are available such as the Cypress CY5676A [77]. BLE would also lower energy consumption demands.

9. A small battery, such as a 150mAh single-cell lithium ion pack, providing persistent power to the main microcontroller and select peripherals would be useful in case of faults with the main battery, or system diagnostics with the main power off. This can be automatically switched with a power mux such as the Texas Instruments' TPS2113A [78] or a diode.
10. The friction-lock connectors chosen for the board were prone to failure after only a few (<20) insertions. Failure is typically non-recoverable as the traces are lifted off the board. To increase reliability, positive-lock connectors should be chosen instead. As a stopgap measure, the connectors can be adhered using glue or epoxy to increase resilience.
11. Future designs should consider independent buck converters for each rail, especially if the power budget is increased with additional on-board logic. This would result in better power efficiency and prevent cascading failure in the event an upstream regulator fails. Alternately, a hybrid approach could be taken which reuses the 12V converter as a primary step-down voltage, then small footprint buck converters used for the 5V (such as the LT1076-5 [79]) and 3.3V rails.
12. The application of conformal coating would increase environmental resistance and protect the electronics against corrosion, dust and moisture.

13. This design is not well suited for partially assistive gait rehabilitation due to the increased bandwidth and processing requirements required. To meet the suggested control loop latency of 1 ms on the feedback channel, additional dedicated RS-485 channels are needed. Alternatively, the servo drives could be substituted with Ethernet/EtherCAT capable models, such as in [80]. The MINDWALKER exoskeleton by Wang et al. is such an example, using a distributed EtherCAT based hardware architecture to implement impedance-control based control system or partial assistance [81].

APPENDIX A: PCB DRC RESULTS AND STACKUP

Table A.1 lists the full DRC output. The one un-routed signal indicated in the results was for a passive decoupling network for the MCU which was internally connected and therefore intentionally not routed on the PCB.

Warnings	Count
Total	0
Rule Violations	Count
Clearance Constraint (Gap=8mil) (OnLayer('Power Plane') or OnLayer('Ground Plane')),(All)	0
Modified Polygon (Allow modified: No), (Allow shelved: No)	0
Net Antennae (Tolerance=0mil) (All)	0
Silk primitive without silk layer	0
Silk to Silk (Clearance=5mil) (All),(All)	0
Silk To Solder Mask (Clearance=5.5mil) (IsPad),(All)	0
Minimum Solder Mask Sliver (Gap=2mil) (Disabled)(All),(All)	0
Hole To Hole Clearance (Gap=5mil) (All),(All)	0
Hole Size Constraint (Min=15mil) (Max=250mil) (All)	0
Height Constraint (Min=0mil) (Max=1000mil) (Preferred=500mil) (All)	0
Width Constraint (Min=10mil) (Max=100mil) (Preferred=10mil) (All)	0
Power Plane Connect Rule(Direct Connect)(Expansion=20mil) (Conductor Width=10mil) (Air Gap=10mil) (Entries=4) (All)	0
Clearance Constraint (Gap=6mil) (InComponent('U?') or InComponent('ANT1')),(All)	0

Un-Routed Net Constraint ((All))	1
Short-Circuit Constraint (Allowed=No) (All),(All)	0
Clearance Constraint (Gap=8mil) (All),(All)	0
Minimum Annular Ring (Minimum=5mil) (All)	0
Total	1

Un-Routed Net Constraint ((All))

Un-Routed Net Constraint: Net NetC6 2 Between Pad U1-25 (1629.842,-2196.457mil) And Pad U1-56 (1629.842,-1753.543mil)

Table A.1: DRC Results (Adapted from Altium Designer Output)

A.1 PCB STACKUP

The full PCB stackup for the Integrated design is shown in Figure A.2.






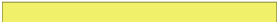





Index	Graphic	Layer	Thickness
1		Top Paste	
2		Top Overlay	
3		Top Solder	0.40mil
4		Component Side	1.40mil
5		2116 x2 TOP	8.00mil
6		Ground Plane	1.42mil
7		Core	40.00mil
8		Power Plane	1.42mil
9		2116 x2 BTM	8.00mil
10		Solder Side	1.40mil
11		Bottom Solder	0.40mil
12		Bottom Overlay	
13		Bottom Paste	
		Total Thickness:	62.43mil (±10%)

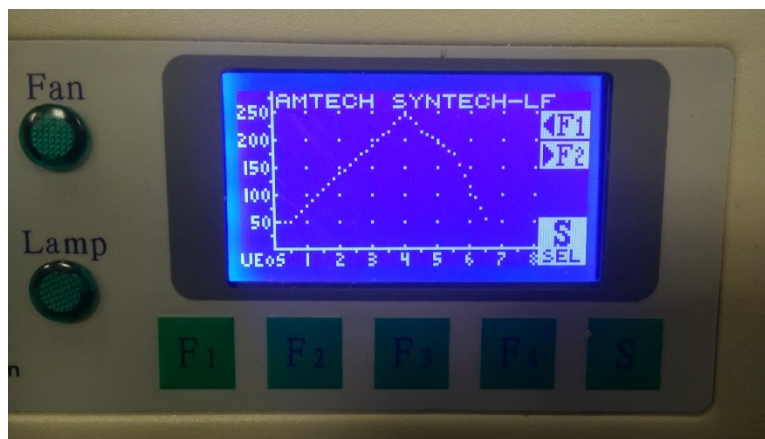
Table A.2: PCB Stackup for Integrated Design

APPENDIX B: IR REFLOW OVEN

The T-962 (Fig. B.1a) is a basic infrared reflow oven with programmable reflow curves. The oven was modified from stock to improve thermal insulation and was flashed with third party firmware by Unified Engineering as per [82] using a standard USB to TTL UART cable. Due to inaccuracies of the thermocouple (biased 12 degrees warm) the default 63-37 reflow profile did not achieve sufficient temperature to reflow the boards. Satisfactory reflows were produced with the default “AMTECH SYNTECH-LF” profile.



(a)

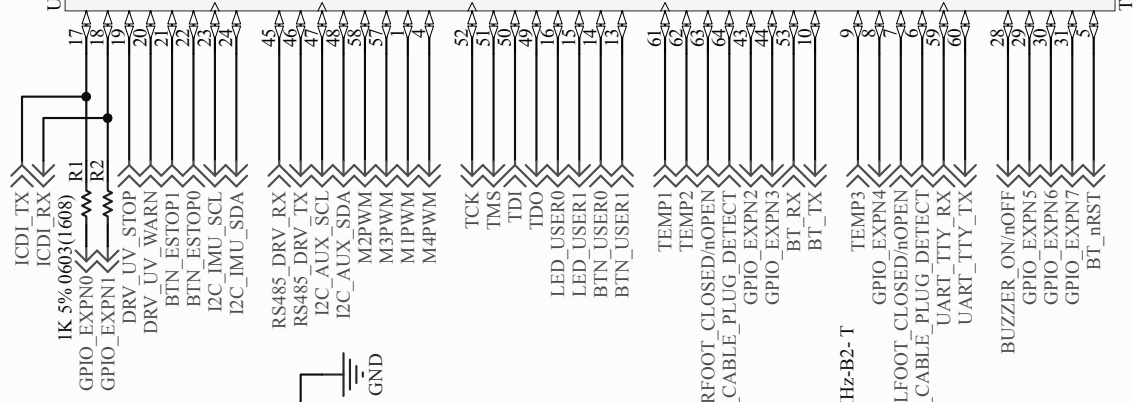
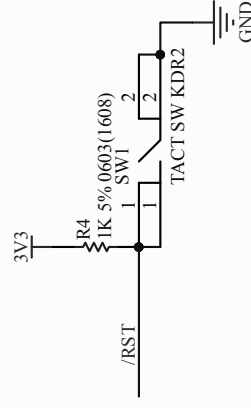
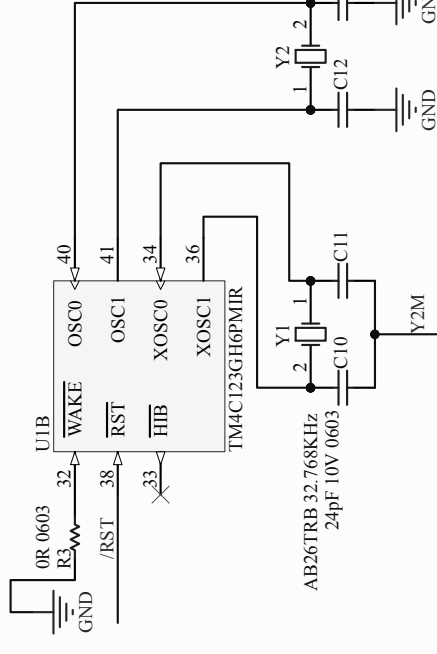
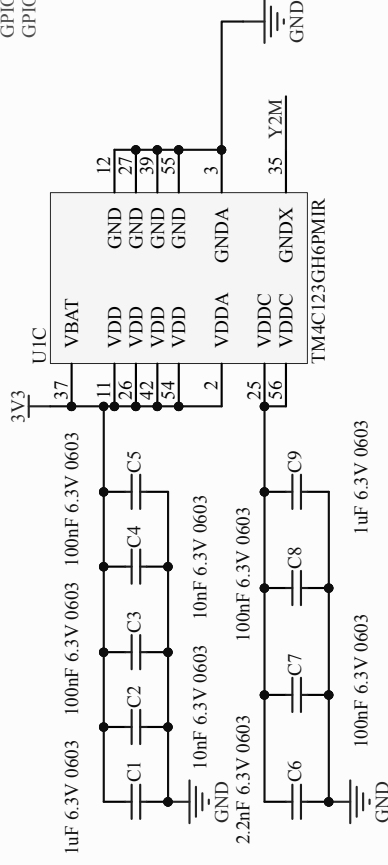


(b)

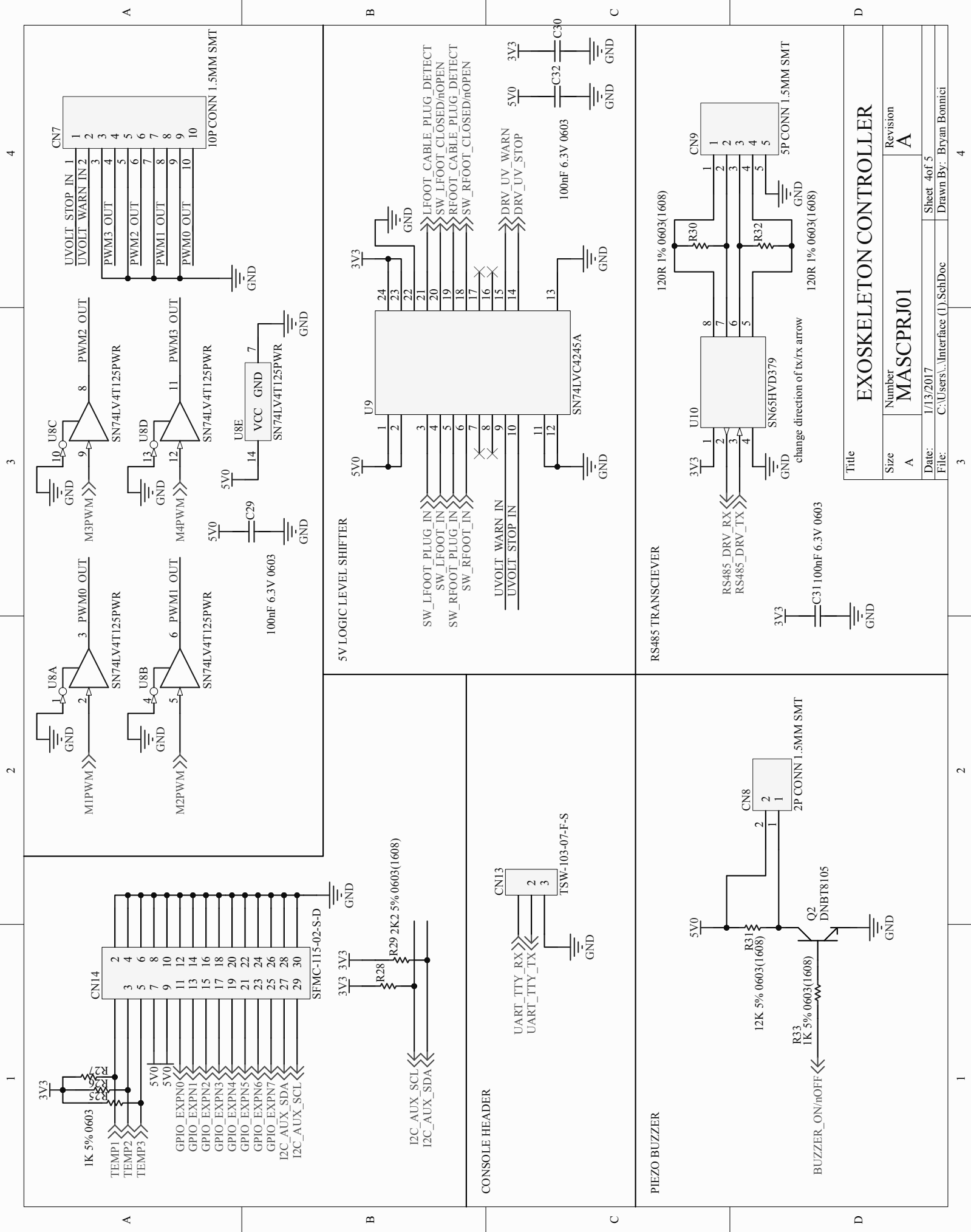
Figure B.1 a) T-962 IR Oven, b) user interface showing reflow profile

APPENDIX C: SCHEMATICS

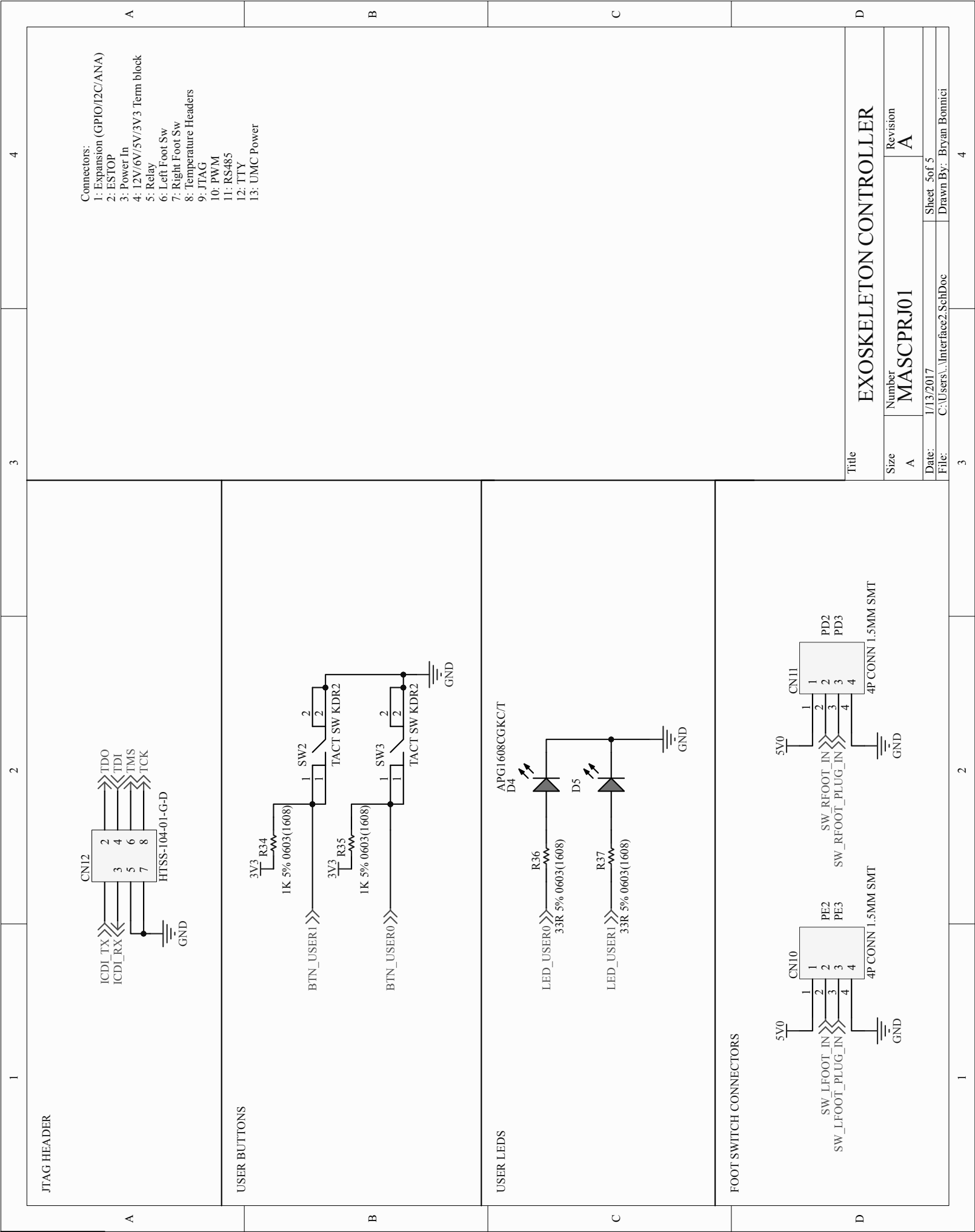
See attached pages.



Title			EXOSKELETON CONTROLLER		
Size	Number	Revision			
A	MASCPRJ01	A			
Date:	1/13/2017	Sheet		1 of 5	
File:	C:\Users\Bryan\Desktop\MCU (1).SchDoc\Drawn Bv: Bryan Bonnici				



Title			EXOSKELETON CONTROLLER		
Size	Number	Revision			
A	MASCPRJ01	A			
Date:	1/13/2017	Sheet 4 of 5			
File:	C:\Users\...\Interface (1).SchDoc	Drawn By: Bryan Bonnici			



REFERENCES

- [1] H. I. Krebs and B. T. Volpe, “Robotics: A Rehabilitation Modality,” *Curr. Phys. Med. Rehabil. Reports*, vol. 3, no. 4, pp. 243–247, 2015.
- [2] M. Talaty, A. Esquenazi, and J. E. Briceno, “Differentiating ability in users of the ReWalkTM powered exoskeleton: An analysis of walking kinematics,” *IEEE Int. Conf. Rehabil. Robot.*, 2013.
- [3] C. K. Thomas, E. Y. Zaidner, B. Calancie, J. G. Broton, and B. R. Bigland-Ritchie, “Muscle weakness, paralysis, and atrophy after human cervical spinal cord injury,” *Exp. Neurol.*, vol. 148, no. 0014–4886 (Print), pp. 414–423, 1997.
- [4] W. T. Phillips *et al.*, “Effect of spinal cord injury on the heart and cardiovascular fitness,” *Curr. Probl. Cardiol.*, vol. 23, no. 11, pp. 641–716, 1998.
- [5] C. S. Fry, M. J. Drummond, H. L. Lujan, S. E. Dicarlo, and B. B. Rasmussen, “Paraplegia increases skeletal muscle autophagy,” *Muscle and Nerve*, vol. 46, no. 5, pp. 793–798, 2012.
- [6] National SCI Statistical Center, “Spinal Cord Injury (SCI) facts and figures at a glance,” Birmingham, AL, 2015.
- [7] T. Anwar, A. Al Jumaily, and S. Member, “System Identification and Damping Coefficient Estimation from EMG based on ANFIS to Optimize Human Exoskeleton Interaction .,” *Fuzzy Syst. (FUZZ-IEEE), 2016 IEEE Int. Conf.*, pp. 844–849, 2016.
- [8] H. I. Krebs *et al.*, “Robot-aided neurorehabilitation: A robot for wrist rehabilitation,”

- IEEE Trans. Neural Syst. Rehabil. Eng.*, vol. 15, no. 1, pp. 327–335, 2007.
- [9] R. L. Harvey, “Improving poststroke recovery: Neuroplasticity and task-oriented training,” *Curr. Treat. Options Cardiovasc. Med.*, vol. 11, no. 3, pp. 251–259, 2009.
 - [10] W. K. Lee and S. Jung, “FPGA design for controlling humanoid robot arms by exoskeleton motion capture system,” *2006 IEEE Int. Conf. Robot. Biomimetics, ROBIO 2006*, pp. 1378–1383, 2006.
 - [11] M. H. Raibert, *Legged Robots that Balance*. Cambridge, MA: The MIT Press, 1986.
 - [12] A. B. Zoss, H. Kazerooni, and A. Chu, “Biomechanical Design of the Berkeley Lower Extremity Exoskeleton (BLEEX),” *IEEE/ASME Trans. Mechatronics*, vol. 11, no. 2, pp. 128–138, 2006.
 - [13] C. J. Walsh, D. Paluska, K. Pasch, W. Grand, A. Valiente, and H. Herr, “Development of a lightweight, underactuated exoskeleton for load-carrying augmentation,” *Proc. - IEEE Int. Conf. Robot. Autom.*, vol. 2006, no. May, pp. 3485–3491, 2006.
 - [14] H. G. Kim, J. W. Lee, J. Jang, C. Han, and S. Park, “Mechanical design of an exoskeleton for load-carrying augmentation,” *2013 44th Int. Symp. Robot. ISR 2013*, 2013.
 - [15] M. Fontana, R. Vertechy, S. Marcheschi, F. Salsedo, and M. Bergamasco, “The Body Extender,” *IEEE Robot. Autom. Mag.*, no. December, pp. 34–44, 2014.
 - [16] J. Murtagh, “ReWalk: Robotic Exoskeletons for Spinal Cord Injury,” *CADTH issues Emerg. Heal. Technol.*, no. 141, 2015.
 - [17] E. Strickland, “Good-bye, wheelchair,” *IEEE Spectr.*, vol. 49, no. 1, pp. 30–32, 2012.
 - [18] Globe Newswire, “FDA Clears Parker’s Indego® Exoskeleton for Clinical, Personal

- Use,” 2016. [Online]. Available: <http://phx.corporate-ir.net/phoenix.zhtml?c=97464&p=irol-newsArticle&ID=2147571>. [Accessed: 10-Aug-2016].
- [19] Brain Products, “Paralyzed man in mind-controlled exoskeleton kicks off FIFA World Cup 2014,” 2014. [Online]. Available: <http://pressrelease.brainproducts.com/fifa-world-cup-2014/>. [Accessed: 30-Jul-2016].
- [20] Globe Newswire, “FDA Clears Parker’s Indego® Exoskeleton for Clinical, Personal Use,” 2016. .
- [21] Ekso Bionics, “Ekso GT™ Robotic Exoskeleton Cleared by FDA for Use With Stroke and Spinal Cord Injury Patients,” 2016. [Online]. Available: <http://ir.eksobionics.com/press-releases/detail/570/ekso-gt-robotic-exoskeletoncleared-by-fda-for-use-with>. [Accessed: 31-Aug-2016].
- [22] ReWalk, “ReWalk Gallery,” 2016. [Online]. Available: <http://rewalk.com/gallery-2/>. [Accessed: 10-Sep-2016].
- [23] L. Kratochwill, “Lightweight Robotic Exoskeleton Approved by FDA,” *Popular Science*, 2016. [Online]. Available: <http://www.popsci.com/indego-exoskeleton-gets-fda-approval>. [Accessed: 10-Aug-2016].
- [24] S. Charara, “This robotic exoskeleton helps patients to walk and it’s getting smarter,” *Wearable*, 2015. [Online]. Available: <https://www.wearable.com/saves-the-day/exoskeleton-paralysed-patients-ekso-bionics-gt-sarah-thomas>. [Accessed: 09-Sep-2016].

- [25] “Ekso Bionics Holdings Inc (NASDAQ:EKSO): Today’s Momentum Play,” *Insider Financial*. [Online]. Available: <https://www.insiderfinancial.com/ekso-bionics-holdings-inc-nasdaqekso-todays-momentum-play/117493/>. [Accessed: 20-Oct-2016].
- [26] J. Rueterbories, E. G. Spaich, B. Larsen, and O. K. Andersen, “Methods for gait event detection and analysis in ambulatory systems,” *Med. Eng. Phys.*, vol. 32, no. 6, pp. 545–552, 2010.
- [27] K. Suzuki, G. Mito, H. Kawamoto, Y. Hasegawa, and Y. Sankai, “Intention-Based Walking Support for Paraplegia Patients with Robot Suit HAL,” *Adv. Robot.*, vol. 21, no. 12, pp. 1441–1469, 2007.
- [28] M. Segar, “Back on his feet,” *Reuters*, 2014. [Online]. Available: <http://blogs.reuters.com/photographers-blog/2014/03/31/back-on-his-feet/>. [Accessed: 02-Jan-2017].
- [29] M. Arazpour, S. W. Hutchins, and M. A. Bani, “The efficacy of powered orthoses on walking in persons with paraplegia,” *Prosthet. Orthot. Int.*, vol. 39, no. 2, pp. 90–99, 2015.
- [30] I. Benson, K. Hart, D. Tussler, and J. J. van Middendorp, “Lower-limb exoskeletons for individuals with chronic spinal cord injury: findings from a feasibility study,” *Clin. Rehabil.*, vol. 30, no. 1, pp. 73–84, 2016.
- [31] J. Kressler *et al.*, “Understanding therapeutic benefits of overground bionic ambulation: Exploratory case series in persons with chronic, complete spinal cord injury,” *Arch. Phys. Med. Rehabil.*, vol. 95, no. 10, pp. 1878–1887, 2014.

- [32] J. B. Nielsen, “How We Walk: Central Control of Muscle Activity during Human Walking,” *Neuroscientist*, vol. 9, no. 3, pp. 195–204, 2003.
- [33] C. L. Vaughan, “Theories of bipedal walking: an odyssey,” *J. Biomech.*, vol. 36, pp. 513–523, 2003.
- [34] S. Shultz, P. Houghlum, and D. Perrin, *Examination of Musculoskeletal Injuries*, Third Edit. Human Kinetics, 2009.
- [35] M. Iosa, A. Fusco, and F. Marchetti, “The Golden Ratio of Gait Harmony: Repetitive Proportions of Repetitive Gait Phases,” *Biomed Res. Int.*, 2013.
- [36] J. Loudon, M. Swift, and S. Bell, *The Clinical Orthopedic Assessment Guide*, Second Edi. Human Kinetics, 2008.
- [37] R. C. Schafer, *Clinical Biomechanics: Musculoskeletal Actions and Reactions*, 2nd Revise. Williams & Wilkins, 1987.
- [38] J. Ahn and N. Hogan, “Walking Is Not Like Reaching: Evidence from Periodic Mechanical Perturbations,” *PLoS One*, 2012.
- [39] J. K. Moore, S. K. Hnat, and A. J. van den Bogert, “An elaborate data set on human gait and the effect of mechanical perturbations.,” *PeerJ*, 2015.
- [40] Y. Iwashita, “Piecewise Polynomial Interpolations,” *OpenGamma*, vol. 15, pp. 1–28, 2013.
- [41] M. Beckerleg and C. Zhang, “Evolving individual and collective behaviours for the Kilobot robot,” *2016 IEEE 14th Int. Work. Adv. Motion Control. AMC 2016*, pp. 263–268, 2016.

- [42] J. Currie, M. Beckerleg, and J. Collins, “Software evolution of a Hexapod Robot walking gait,” *15th Int. Conf. Mechatronics Mach. Vis. Pract. M2VIP’08*, pp. 305–310, 2008.
- [43] Boston Dynamics, “BigDog Overview,” *Boston Dynamics*. p. 22, 2008.
- [44] D. K. Yoon, S. Y. Kim, J. Cho, K. K. Lee, and B. J. You, “Development of a compact motor controller supporting EtherCAT for a dual-arm telepresence robot,” *2014 11th Int. Conf. Ubiquitous Robot. Ambient Intell. URAI 2014*, no. Urai, pp. 253–256, 2014.
- [45] S. Jorg, J. Tully, and A. Albu-Schaffer, “The Hardware Abstraction Layer - Supporting control design by tackling the complexity of humanoid robot hardware,” *Proc. - IEEE Int. Conf. Robot. Autom.*, pp. 6427–6433, 2014.
- [46] B. Siciliano, L. Sciavicco, and L. Villani, *Robotics: Modelling, Planning and Control*. Springer London, 2009.
- [47] T. R. Kurfess and J. S. Falcon, “Sensors and Actuators,” in *Robotics and Automation Handbook*, Boca Raton, FL: CRC Press, 2005, pp. 240–242.
- [48] University of California Berkeley, “ME102 Lab 4: RC Servo.” [Online]. Available: <http://courses.me.berkeley.edu/ME102B/lab4.html>. [Accessed: 10-Sep-2016].
- [49] Bionik Laboratories, “ARKE Gen 2.0 User Manual Version 2.”
- [50] Texas Instruments, “Tiva™ TM4C123GH6PM Microcontroller,” Dallas, 2014.
- [51] Texas Instruments, “TI-RTOS: Real-Time Operating System (RTOS) for Microcontrollers (MCU).” [Online]. Available: <http://www.ti.com/tool/ti-rtos-mcu>. [Accessed: 01-Nov-2016].
- [52] Texas Instruments, “Getting Started with the TIVA™ C Series TM4C123G LaunchPad,”

2016. [Online]. Available:
http://processors.wiki.ti.com/index.php/Getting_Started_with_the_TIVA%E2%84%A2_C_Series_TM4C123G_LaunchPad. [Accessed: 06-Sep-2016].
- [53] Roving Networks, “RN41XV & RN42XV Bluetooth Module.”
 - [54] Linear Technology, “RS485 Quick Guide,” p. 1.
 - [55] Texas Instruments, “RS-485 Reference Guide,” Dallas, 2014.
 - [56] Texas Instruments, “Tiva™ C Series TM4C123G LaunchPad Evaluation Board User’s Guide,” Dallas, 2013.
 - [57] M. N. O. Sadiku, *Elements of Electromagnetics*, 5th ed. New York, 2010.
 - [58] D. M. Hockanson, X. Ye, J. L. Drewniak, T. H. Hubing, T. P. Van Doren, and R. E. DuBroff, “FDTD and experimental investigation of EMI from stacked-card PCB configurations,” *IEEE Trans. Electromagn. Compat.*, vol. 43, no. 1, pp. 1–10, 2001.
 - [59] H.-H. Chou and Y.-S. Lee, “Experimental investigation and analysis of EMI in stacked I/O connectors of PCB,” *J. Electromagn. Waves Appl.*, vol. 30, no. 2, pp. 195–206, 2016.
 - [60] C. Cham and Z. Bin Samad, “Brushless DC Motor Electromagnetic Torque Estimation with Single-Phase Current Sensing,” vol. 9, 2014.
 - [61] Texas Instruments, “Understanding the Terms and Definitions of LDO Voltage Regulators,” Dallas, 1999.
 - [62] Texas Instruments, “LM3940 1A Low-Dropout Regulator for 5V to 3.3V Conversion Output Voltage,” Dallas, 2015.

- [63] Texas Instruments, “LM340 , LM340A and LM7805 Family Wide VIN 1.5-A Fixed Voltage Regulators,” Dallas, 2016.
- [64] Texas Instruments, “LM317A 1 % Accurate Three-Terminal Adjustable Regulator,” Dallas, 2015.
- [65] Texas Instruments, “LM5010 High-Voltage 1-A Step-Down Switching Regulator,” Dallas, 2016.
- [66] Texas Instruments, “LM5010 High-Voltage 1-A Step-Down Switching Regulator,” Dallas, 2016.
- [67] A. Weiler and A. Pakosta, “High-Speed Layout Guidelines,” *Application Report, SC4A082*, no. November. Texas Instruments, pp. 1–20, 2006.
- [68] Texas Instruments, “SN74LVC4245A Octal Bus Transceiver and 3 . 3-V To 5-V Shifter With 3-State Outputs,” Dallas, 2015.
- [69] Texas Instruments, “SN74LV4T125 Single Power Supply Quadruple Buffer Translator GATE With 3-State Output CMOS Logic Level Shifter,” Dallas, 2014.
- [70] R. Baldwin, S. Bobovych, R. Robucci, C. Patel, and N. Banerjee, “Gait analysis for fall prediction using hierarchical textile-based capacitive sensor arrays,” *2015 Des. Autom. Test Eur. Conf. Exhib.*, pp. 1293–1298, 2015.
- [71] S. Schutz, K. Mianowski, C. Kotting, A. Nejadfard, M. Reichardt, and K. Berns, “RRLab Sea - A Highly Integrated Compliant Actuator with Minimised Reflected Inertia,” in *2016 IEEE International Conference on Advanced Intelligent Mechatronics (AIM)*, 2016, pp. 4–9.

- [72] T. Desplenter, J. Lobo-Prat, A. H. A. Stienen, and A. L. Trejos, “Extension of the WearME framework for EMG-driven control of a wearable assistive exoskeleton,” *IEEE/ASME Int. Conf. Adv. Intell. Mechatronics, AIM*, vol. 2016–Septe, pp. 288–293, 2016.
- [73] M. Lancini, M. Serpelloni, S. Pasinetti, and E. Guanziroli, “Healthcare Sensor System Exploiting Instrumented Crutches for Force Measurement during Assisted Gait of Exoskeleton Users,” *IEEE Sens. J.*, vol. 16, no. 23, pp. 8228–8237, 2016.
- [74] Health Canada, “LIMITS OF HUMAN EXPOSURE TO RADIOFREQUENCY ELECTROMAGNETIC ENERGY IN THE FREQUENCY RANGE FROM 3 KHZ TO 300 GHZ - SAFETY CODE 6,” 2015.
- [75] Health Canada, “List of Recognized Standards for Medical Devices,” 2016. [Online]. Available: http://www.hc-sc.gc.ca/dhp-mps/md-im/standards-normes/md_rec_stand_im_norm_lst-eng.php. [Accessed: 09-Dec-2016].
- [76] Bluetooth SIG, “Security, Bluetooth Smart (Low Energy),” 2015.
- [77] Cypress Semiconductor, “CY5676A P_{RoC}TM BLE 256KB Module with Bluetooth 4.2 Radio.” [Online]. Available: <http://www.cypress.com/documentation/development-kitsboards/cy5676a-proc-ble-256kb-module-bluetooth-42-radio-0>. [Accessed: 31-Aug-2016].
- [78] Texas Instruments, “TPS2113A - Autoswitching Power Mux,” Dallas, 2012.
- [79] Linear Technology, “LT1076-5 - 5V Step-Down Switching Regulator,” pp. 1–8.
- [80] Elmo Motion Control, “Gold Digital Servo Drives,” 2016. [Online]. Available:

<http://www.elmomc.com/products/gold-digital-servo-drives-main.htm>. [Accessed: 09-Dec-2016].

[81] S. Wang *et al.*, “Design and Evaluation of the Mindwalker Exoskeleton,” *Ieee Trans. Neural Syst. Rehabil. Eng.*, vol. 23, no. 2, pp. 277–286, 2015.

[82] UnifiedEngineering, “T-962 Improvements,” *GitHub*. [Online]. Available: <https://github.com/UnifiedEngineering/T-962-improvements>. [Accessed: 31-Aug-2016].

GLOSSARY

0603 – An SMD with a footprint measuring .006” x .003”
12V0 – 12.0V
3V3 – 3.30V
5V0 – 5.0V
A – Amp or Ampere
ARM – Advanced RISC Machine, a family of microcontroller architectures
BLDC – Brushless DC
BOM – Bill of Materials
C – Capacitor
CAD – Computer Aided Design
DC – Direct Current
DMM – Digital Multimeter
DOF – Degree of Freedom
DRC – Design Rules Check
FBE – Full Body Exoskeleton
FR4 – A glass epoxy used as a common PCB material
GPIO – General Purpose Input Output
I2C (or I²C) – Inter-Integrated Circuit, a serial computer bus used for low speed peripherals
IMU – Inertial Measurement Unit, a device which measures forces and/or orientation.
IO – Input Output (see also GPIO)
LUT – Lookup Table
Hz – Unit of frequency
JTAG – Joint Test Action Group (also a common interface for programming microcontrollers)
LED – Light Emitting Diode
MCU – Microcontroller Unit
MEMS – Microelectromechanical systems
MIPS – Millions of Instructions Per Second, a unit of embedded performance
P[X][#] e.g. PC4, PD5 – A port identifier on a microcontroller
PCB – Printed Circuit Board
PID – Proportional Integral Derivative
PWM – Pulse Width Modulation
R – Resistor
RX - Data Receive
SCI – Spinal Cord Injury
SDK – Software Development Kit
SMD – Surface Mount Device
SPP – Serial Port Profile
TH – Through Hole
TX – Data Transmit
UART – Universal Asynchronous Receiver Transmitter
V – Volt or Voltage
VDD – The positive power supply of a CMOS circuit